Universität Stuttgart

Baustatik und Baudynamik

ISOGEOMETRIC SHAPE OPTIMIZATION OF BEAM WITH LARGE DEFORMATIONS

Masterarbeit

vorgelegt von

Ayan Haldar

im

September 2013

Institut für Baustatik und Baudynamik
Prof. Dr.-Ing. habil. Manfred Bischoff

Isogeometric Shape Optimization of Beam with Large Deformations

Master Thesis by
Ayan Haldar

Supervisors:

Dr. Fehmi Cirak
Prof. Dr.-Ing. habil. Manfred Bischoff

Universität Stuttgart

Institut für Baustatik und Baudynamik
Prof. Dr.-Ing. habil. M. Bischoff

September 2013

Erklärung

Hiermit erkläre ich, dass ich die hier vorliegende Bachelorarbeit selbständig verfasst habe. Es wurden nur die in der Arbeit ausdrücklich benannten Quellen und Hilfsmittel verwendet. Wörtlich oder sinngemäß übernommenes Gedankengut habe ich als solches gekennzeichnet. Die eingereichte Arbeit war und ist weder vollständig noch in wesentlichen Teilen Gegenstand eines anderen Prüfungsverfahrens. Ebenso habe ich die Arbeit weder vollständig noch in Teilen bereits veröffentlicht. Ich versichere, dass das elektronische Exemplar mit den anderen Exemplaren übereinstimmt.

Stuttgart, September 15, 2013 _____

Abstract

Design optimization has become one of the most important topics in various engineering sectors. It has become a major challenge for an engineer to develop the best possible design keeping necessary constraints in mind. If mathematical model for optimization is developed carefully incorporating all necessary design variables and with sufficient accuracy, optimized design promises to bring improved designs than that are followed for years. The growth of this field is closely related to the development of computer capabilities, numerical techniques and geometric modelling. However, it has been always been the foremost goal for integrating all these related fields into a single package. So, whenever a designer sits to design any product, he/she should have all the necessary tools namely modelling, analysis and optimization all together. Until the development of isogeometric analysis, this has been a formidable task.

Isogeometric analysis is a computational method that uses the same geometrical representation as used in Computer Aided Design. It not only provides an accurate modelling of complex geometries but also allows refinement procedure in the CAD representation of the geometry. This idea of this thesis is to further extend this concept in integrating with optimization model. As a result, geometric representation used for isogeometric analysis could be included into the optimization model, thus making it possible to merge CAD, FEM and optimization process.

Most of the optimization models used in industry is limited to linear sensitivity analysis, which is not accurate for structures involving geometric nonlinearity. Most of them also use parameterized optimization which has the disadvantage of restricting the design variable space. In this present model, a numerical formulation is presented for nonparametric shape optimization using isogeometric formulation that allows easy integration of CAD, FEM and an optimization strategy that combines nonlinear path following methods with the design changes during the optimization procedure. The adjoint sensitivity method is used to reduce the numerical effort as in this problem design variables are much larger than the constraint equations. The mechanics of the beam is described by using a similar model of thin shells, so that this formulation could be easily extended to thin shell models.

With the development of such model, it is possible to augment existing nonlinear finite element analysis codes to calculate design sensitivity of response variables accounting even for geometric nonlinearity.

Acknowledgement

This master thesis is the result of my work at the Computational Structural Mechanics Lab, Department of Engineering, University of Cambridge, UK, between March 2013 to August 2013.

I would like to sincerely thank Dr. Fehmi Cirak for giving me the opportunity to work in his research group and for his helpful guidance and support as my supervisor.

Furthermore, I would like to address my thanks to all the members of the Computational Structural Mechanics Lab for some fruitful discussions. Especially, I would like to thank Kosala Bandara, for his engagement and constructive ideas.

I am indebted to Prof. Dr.-Ing. Manfred Bischoff for being my internal mentor at University of Stuttgart and for his guidance and support. I would also like to thank Dr.-Ing Malte Von Schevan for helping me out during the compilation of the report.

I am thankful to my parents and friends for their constant love and support.

Finally, I gratefully acknowledge the Erasmus Mundus scholarship given by the European Union during this whole Masters programme.

Stuttgart, in September 2013 Ayan Haldar

Contents

List of Figures

List of Tables

1

Introduction

1.1 Motivation

Over the years, engineers have attempted to improve design of various structural components. Methods like Edisonian approach were implemented for several years by means of trial and error method. However, these methods were mostly based on intuition or experience, with very less knowledge of improvement by mathematical means. With the increase in computer power and capacity, there came a scope of developing numerical techniques for optimizing design. In order to reduce design time and cost, automated design optimization held a special place for the improvement of engineering design. With Finite Element Methods coming into its role, structural differential equations could be solved more efficiently and with better accuracy. As, for structural optimization, a flexible and robust method is needed to describe structural properties, which is very well supported by the finite element framework. This also brings the possibility of augmenting existing Finite Element codes with various structural optimization schemes. Thus with its tremendous application in civil, aeronautical, mechanical engineering, structural optimization promises much improved designs saving a significant amount of material, cost and time.

However, even after years of research, the use and scope of structural optimization is limited to only certain areas of engineering design. Its lack of use is mainly because of reasons like:

1. It may be difficult, to formulate one or more simple performance criteria for optimization. The designer must be able to clearly define quantifiable objective function, and identify all important constraints.

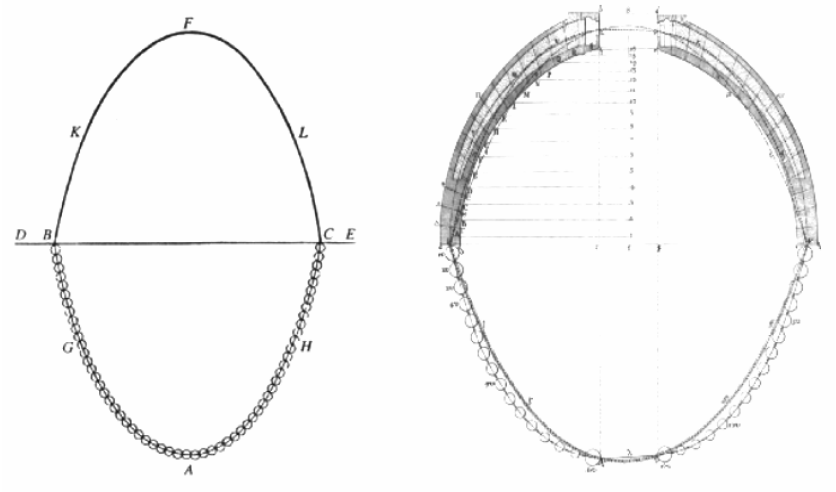

Figure 1.1: (a) Poleni's drawing of Hooke's analogy between an arch and a hanging chain, and (b) his analysis of the Dome of St.-Peter's in Rome [1748] (Block et al. (2006))

2. Usually in commercial optimization packages, the sensitivities are calculated using global finite difference or semi analytical method which are mostly computationally expensive and not very accurate.

3. Mostly the formulations are limited to linear static sensitivity analysis which is inaccurate and doesn't produce efficient shapes for nonlinear problems which are quite common in industry.

4. Most of the commercial software contains paramametrized optimization, which doesn't include the full design space and is restricted to prior definition of design elements whereas, representation with nonparametrized optimization includes all possible solutions of the design space.

Therefore, there is a need to develop a robust formulation for nonparametric shape optimization that could be extended to geometrically nonlinear problems. In this thesis work, thus a numerical formulation is presented for shape optimization of beams with large deformation in a parameterized free space. The mechanics of beam is described in a similar way as it is done for shell structures, so that the sensitivities could be easily extended for thin shell problem.

1.2 Historical Background

In the past, a lot of architects and engineers have developed various methods for obtaining shape optimized design. In 1675, Hooke stated that 'As hangs the flexible chain,

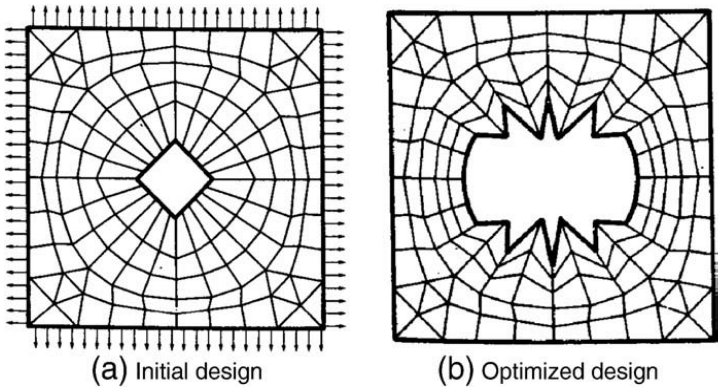

Figure 1.2: Optimized shape of a hole in a plate where elements nodes are used as design variables. Figures are taken from Braibant and Fleury (1984).

so but inverted will stand the rigid arch' as quoted in Heymann (1995), which was famously referred as inverted catenary theorm. The idea of the inverted catenary theorm became quite popular in designing many civil engineering structures. It was applied by Polini to prove Saint Peters stability as shown in Fig 1.1 and Antonio Gaudi's work in several masonary compression structure. Architect Frei Otto created forms of greatest structural efficiency and minimum use of materials. The extensive review of historical use of various methods and their application in comtemporary architecture could be found in Larena (2009,Cottbus). For two dimensional structure, Isler (2000) extensively used this concept in various problems. These primary concepts of these shape optimal design could be taken into use as verification problems even with gometrical nonlinear problems.

The development of shape optimization in a general form was first proposed by Zienkiewicz and Campbell (1973). In their work, the design variable was taken as the nodal coordinates which most intuitive and directly relates finite element. However, serious drawbacks were found by Haftka and Grandhi (1986). They showed through an optimization problem where the objective was to find the shape of the hole that minimizes the total weight and for which the stresses in the boundary hole elements do not exceed a given allowable value (Figure 1.2). It is quite clear from Figure 1.2 that optimized result produced some wriggly shapes leading to impractical designs.

Thus, in order to attain smooth boundary design, it was important to separate design model with finite element model. Various researchers, therefore described the design model by polynomial type functions like used by Pedersen and Laursen (1983) However, polynomial representation ensured some boundary smoothness but generated oscillations when the polynomial degree was too high. Moreover, it was difficult to generate any arbitrary curve. Usually it could only represent curves like quadratic, cubic etc. falling under a particular family. It was also difficult to control the curve locally, like

changing a single polynomial point would affect the whole geometry, which was not very much desired by the designers. Therefore, in order to eliminate these problems, the B-Spline curves were used for shape optimization. Braibant and Fleury (1984) showed how B-Splines could be used to overcome difficulting dealing with complex shape. Not only it guaranteed smoothness of curve, but it also had good local control. The design variable was taken as the control point coordinates, rather than nodal coordinates. This became a very handy tool for various shape optimization problems. Later, Non Uniform Rational B-Splines were used to describe the shape of the structures by Schramm and Pilkey (1993), although the displacement response was approximated by p-version of finite element method.

The industrial problems are usually in the form of CAD model, which can be effectively linked with finite element model using isogeometric concepts and can effectively transfer information smoothly back. There is challenge therefore, to successfully allow easy flow of information between the finite element model and optimization model, and back to the CAD model. Figure 1.3 depicts the integration model with isogeometric model. This integration will bring the analysis using FE and optimization available to a design engineer into a single package, and allow smooth flow of information between the triads: design, analysis and optimization.

Recently, few researchers have used the concept of isogeometric shape optimization. Wall et al. (2008) discussed the shape optimisation of planar elasticity problems. Though the set of design variables only consisted of the control point co-ordinates, the validity and efficiency of the approach has been verified also for knot vectors of repeated internal knots. Cho and Ha (2009) introduced isogeometric shape optimization, where the geometrical properties of design were embedded in the NURBS basis function and the changes in control points resulted in shape design. Since the geometry is exactly encapsulated at the design level, mesh refinement and representation of shape changes are more easily obtained. Therefore, during the optimization process, without the need of communicating back to CAD model, design modification of complex structures could be performed. Instead of taking just the control points as design variables, Qian (2010) presented an approach for the analytical sensitivity with both position and weights of the control points as design variable.

Similarly, not only NURBS, lot of researchers have used other discretization techniques for calculating shape sensitivities. Optimized design was found out by using subdivison surfaces by Cirak et al. (2002). More recently, Ha et al. (2010) proposed the application of T-spline for more efficient computation of shape optimal designs.

In the research discussed so far, most of them were limited to the linear regime of the structure response. Structural optimization of geometrically nonlinear models incor-

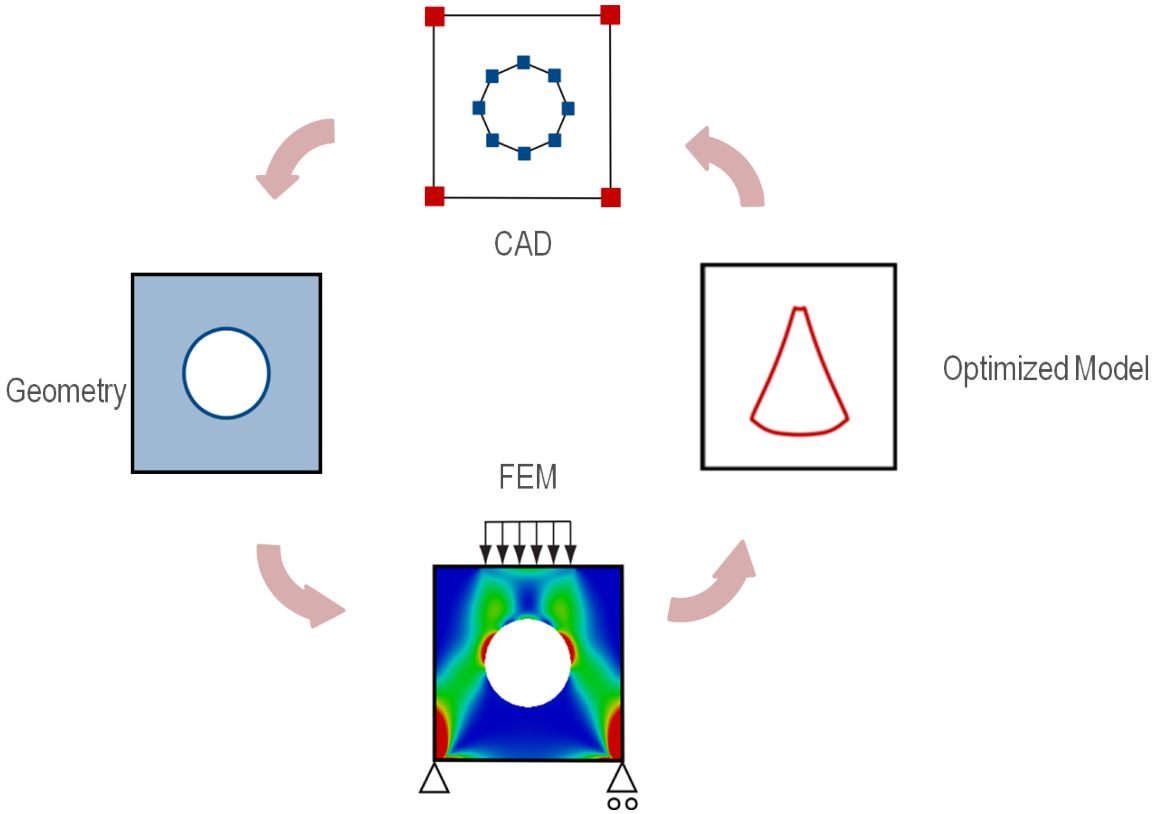

Figure 1.3: Integration of CAD, FEM and Optimization model

porates the nonlinear behaviour in the structure while also performing the sensitivity analysis. Though, many researchers have made attempts to use nonlinear structural analysis for structural optimization in the past, only some have successfully developed model using CAD integration. Santos and Choi (1992) derived shape design sensitivities of nonlinear structural systems using the continuum approach. For topology optimization, design sensivities were found out for displacement load nonlinear structures by Cho and Jung (2003), where again he continuum based sensitivity method was used. More recently, parameterized shape optimization of nonlinear structures using discrete method was done by Firl (2010). The computational cost was significantly lowered by taking triangular approximation for nonlinear response function. However, very less number of sample points in the integration of the nonlinear curve decreases the accuracy of the nonlinear problem. Except few, most of the research done on structural optimization on nonlinear structures are based on continuum approach and with parametric design space.

1.3 Thesis Layout

This thesis is organized into seven chapters. Following the motivation and short literature review, various types of structural optimization is presented in Chapter 2. The difference in size, shape and topology optimization is also explained briefly.

The isogeomteric concepts are briefly explained in Chapter 3. As, in the present work, uniform B-splines have been used, its definition, the concept of knot vector and description of basis vector are presented.

Chapter 4 describes the formulation of the beam element used. The presented formulation is quite similar to the shell formulation by Cirak et al. (2000) used for subdivision shell, with some assumptions valid for Euler-Bernoulli beam.

Chapter 5 follows with the description of various types of sensitivity analysis techniques used in structural optimization. Comparison between various techniques are made, with its applicability.

In Chapter 6, the nonlinear analytical sensitivity is derived using adjoint technique. The objective function is taken as the strain energy with the goal of minimizing it. Sensitivity analysis of various components are derived one by one in a systematic way.

In Chapter 7, some simple problems of linear and nonlinear beam are taken and analyzed using isogeometric concepts. Later, shape optimization of simple beam problems are taken and compared with the catenary curve theorm. Some investigations are made on the effect of optimal shape on changing parameters, like load, mesh size and length by thickness ratio.

In Chapter 8, the thesis concludes with a brief summary of the thesis work and an algorithm of the whole implementation is presented. Some possible extension of the current work is also suggested.

2

Structural Optimization

This chapter introduces the basic terminologies and concepts in structural optimization. The objective function and the constraints of the optimization problem are defined. Using the Lagrangian function, the objective function and the constraints are reformulated into a single function. In order to define the optimality condition of the Lagrangian function, the Karush-Kuhn-Tucker Condition (KKTC) is also presented. Further, the basic classes of defining optimization problem namely size, shape and topology are explained briefly.

As, optimization in general is a method of finding the best of all possible solutions. Therefore, structural optimization aims at finding the best structural design within the given design space and satisfying necessary constraints. However the term best is quite generic. In order to define some goals, *objective functions* are defined. This can be minimizing weight, displacement, energy etc. Therefore, a well defined objective function is necessary to formulate a optimization problem. The objective function must be choosen such that it could be easily defined in terms of mathematical functions. These objective functions depend on certain variables, which is changed in order to achieve the goal of the optimization problem. They are known as *design variables*. They can be nodal coordinates, thickness, fiber angles etc. Next, in order to solve an optimization problem, it is necessary to define some *constraints*. This defines a range where the optimization algorithm, will restrict the design variables to solve the problem. In order words, a feasible domain to attain an acceptable design. Clearly, there can be both *equality* and *inequality* constraints. In some structural optimization problems, the design space is restricted in order to attain desired shape. This can be parameters that define a well defined geometry, density etc. But, restricting the design space doesn't always result in a global minimum. However, the results are more visually pleasing in this case, and are more ready to use for industrial design problems. In this thesis work,

however, nonparametric design space is considered for the optimization problem, where the full design space is taken into account.

With these definitions in mind, the optimization problem would be therefore written as:

$$\begin{aligned} &\text{Minimize: } \psi(\mathbf{s},\mathbf{u}(\mathbf{s})), \mathbf{s} \in \mathbb{R}^{n_s} \\ &\text{Subject to:} \\ &\qquad g(\mathbf{s},\mathbf{u}(\mathbf{s})) \leq 0 \\ &\qquad h(\mathbf{s},\mathbf{u}(\mathbf{s})) = 0 \\ &\qquad s_{min} \leq \mathbf{s} \leq s_{max} \end{aligned} \tag{2.1}$$

Objective function is defined as ψ which is function of the vectors of design variables and state variables i.e displacements, with the goal of minimizing it. The values of design variable are limited to s_{min} and s_{max}. Equality constraint g and inequality constraint h must be followed as well. The usual technique for performing optimization of such problems is as follows:

1. Starting with a initial guess of design variables, the value of the objective function is evaluated. Finite element method is used in order to achieve this in structural optimization problems.
2. The sensitivity of the objective function to the changes in the design variables is evaluated. This is referred as the design sensitivity analysis and is usually done calculating the gradients of objective function and constraints.
3. Using mathematical optimization techniques like SQP, interior point, MMA etc. the values of design variables are changed. Step 1-3 is repeated until the optimized values are found. In this thesis work, the MATLAB predefined function called *fmincon* is used for the optimization algorithm. Specifically,the interior point method was used in this thesis work.

2.1 Karush-Kuhn-Tucker Conditions

In small scale optimization problem, the objective function could be written in the form of design variables explicitly. However, problems including nonlinearity don't have exact analytical expression of the objective function written in terms of the design variables. In such cases, the objective function is a implicit function of the design variables, as in Equation 2.1. $\mathbf{u}$ is also a function of $\mathbf{s}$ but its not possible to find an analytical expression of $\mathbf{u}$ with terms to $\mathbf{s}$ for a nonlinear problem. Here, the value of $\mathbf{u}$ is found through numerical iterative procedures. Optimization involving such objective functions are usually nonconvex in nature. Therefore, there is always difficulty solving such problems.

The Karush-Kuhn-Tucker Condition(KKTC) is a powerful method for solving constrained optimization. Through this method, the extremum of a function consisting of several variables is found, satisfying the constraint equations. For nonconvex problems, these are used as necessary but not sufficient conditions. In order to write the KKT conditions, first the lagrangian function needs to be defined:

$$L(\mathbf{s},\, \mathbf{u},\, \boldsymbol{\lambda},\, \boldsymbol{\mu}) = f(\mathbf{s},\mathbf{u}) + \sum_{i=1}^{n^g} \lambda_i \cdot g_i(\mathbf{s},\mathbf{u}) + \sum_{j=1}^{n^h} \mu_j \cdot h_j(\mathbf{s},\mathbf{u}); \quad \lambda_i > 0, \mu_j \neq 0 \tag{2.2}$$

here $\boldsymbol{\lambda}$ and $\boldsymbol{\mu}$ are called the dual variables, and $\mathbf{s}$ as the primal variable. $\boldsymbol{\lambda}$ and $\boldsymbol{\mu}$ measures the change of objective functions with respect to the equality and inequality constraints. The KKTC conditions are the extension of Lagrangian Multiplier Method that can be used also for inequality constraints. This is how the conditions look:

$$\nabla_{\mathbf{s}} f(\mathbf{s},\mathbf{u}) + \sum_{i=1}^{n^g} \lambda_i \nabla_{\mathbf{x}} g_i(\mathbf{s},\mathbf{u}) + \sum_{j=1}^{n^h} \mu_j \nabla_{\mathbf{x}} h_j(\mathbf{s},\mathbf{u}) = 0 \tag{2.3}$$

$$\lambda_i \nabla_{\lambda_i} L(\mathbf{s},\, \mathbf{u},\, \boldsymbol{\lambda},\, \boldsymbol{\mu}) = \lambda_i g_i(\mathbf{s},\mathbf{u}) = 0 \tag{2.4}$$

$$\nabla_{\mu_j} L(\mathbf{s},\, \mathbf{u},\, \boldsymbol{\lambda},\, \boldsymbol{\mu}) = \lambda_i g_i(\mathbf{s},\mathbf{u}) = 0 \tag{2.5}$$

$$\lambda_i \geq 0 \tag{2.6}$$

2.2 Types of Size Optimization

2.2.1 Size Optimization

Historically most of the structural optimization problems were based on size optimization. Typically, the design variables include thickness, width or moment of inertia, or other cross sectional parameters. This is easier to implement as the Finite Element mesh is affected by the change in design variables. Therefore, integration with FE mesh and design variables is not required. An example of size optimization problem would be minimization of cross section area of the truss member.

2.2.2 Shape Optimization

In this case, the design variable includes the form or contour of the boundary that define the shape of the structural domain. Usually the design variables consist of nodal coordinates or the control points of the CAD model. For shape optimization, the complexity increases due to its dependency on finite element mesh and also it is more expensive to

calculate the analytical sensitivities. However, most of the problems in shape optimization results in more effective results than size optimization. For example, in problem presented in the introductory chapter (Fig 1.3), the size optimization would result in change in thickness of the plate whereas shape optimization would result in change in shape of the hole.

2.2.3 Topology Optimization

In topology optimization, the optimized connectivity of the domain and material layout is found. Usually, the material density is taken as design variable. The variable takes either value 0 or 1, and thus the optimized material layout of the structure is obtained, consisting of optimal location of the material points and voids. For thin structures, the topology concepts could be applied to attain a truss like structures.

3

Shape Representation

As discussed in Chapter 2, coordinates of certain structural nodes can be selected as design variables for shape optimization problem. But, for complex geometries and fine mesh, the number of design variables tends to be very high. In order to allow smooth and efficient solution, the number of design variables should be kept as small as possible but still allowing enough freedom for general shape. This could be achieved by representing the shape evolution by B-Splines. This method consisits in dividing a curve of data into certain number of segments, each one being defined by polynomials of B-Spline, and to these segments to form a made up curve. The connection of the segments is made by observing conditions of continuity to control nodes. Any modification of the control point results only in the local change of the curve, as not disturbing it globally. Even complex geometries are accurately represented using B-Spline. Remeshing techniques are also easy without any need to communicate again with the CAD enviroment. For some of these reasons, B-Splines are quite ideal for using in optimization problems.

As for shape optimization, the nodal sensitivities, i.e. the partial derivatives of the nodal positions with respect to the design variables are needed. These sensitivities will depend on how the shape is represented and also on how the finite element mesh is generated. This chapter presents a short description of Uniform B-Spline, its basis function and knot vectors.

3.1 Definition

For smooth functions, polynomial approximations provide reasonable accuracy. However, this may not be possible with large interval sizes. Changing a polynomial point also has a global influence, which is not desirable. Therefore, it is natural to use functions

that are piecewise in nature. Clearly, construction of a local basis is the key to efficient numerical treatment. A B-Spline curve contains appropriate local basis function, and is defined by divided difference of truncated power function of certain degree. It is more complex than the Bezier curves, but allows local control of the shape. It is defined by a specific set of coordinates called the control points. However, the degree of the curve is not dependent on the the number of control points.

The B-Spline curve is defined by:

$$\mathbf{Q}(u) = \sum_{j=0}^{n} \mathbf{P}_j B_{j,d}(u) \qquad (3.1)$$
$$t_{d-1} \leq t_{n+1}$$

where P_j is a control point. j is the index of control points. $n+1$ is the number of control points, d is the number of the control points that control a segment. Implying $d-1$ is the degree of the polynomial, for example: $d=2$ is linear, $d=3$ is quadratic, $d=4$ is cubic etc. The value of n must be larger or equal to d. t_j is the knot value. A few knot values form a knot vector $\mathbf{t}$.

3.1.1 B-Spline's Basis Function

There are two mathematical definition of B-Spline's basis function: when $d=1$ and when $d>1$. These two definitions depend on the knot vector $\mathbf{t}$, where $\mathbf{t} = (t_0, t_1, t_2, \ldots)$. The basis vector are defined by the Cox-de Boor recursion formula: When $d=1$

$$B_{j,d}(u) = \begin{cases} 1 \; if \; t_j \leq u \leq t_{j+1} \\ 0 \; otherwise \end{cases} \qquad (3.2)$$

When $d>1$

$$B_{j,d}(u) = \left(\frac{u - t_j}{t_{j+d-1} - t_j} B_{j,d-1}(u) \right) + \left(\frac{t_{j+d} - u}{t_{j+d-1}} B_{j+1,d-1}(u) \right) \qquad (3.3)$$

3.1.2 Knot Vector

Each curve segment is divided into $n+d$ intervals by some values for u called the knot vector. As can be observed in the last two equations, the knot vectors affects the values of the basis function. Moreover, different ways to build the vector create two different

types of B-Splines: **uniform** and **non-uniform**. The number of the knot values(or the size of the knot vector is determined by:

$$m = n + d + 1; \tag{3.4}$$

Hence, if $n = 2$ and $d = 2$ then $m = 5$, $\mathbf{t} = (t_0,t_1,t_2,t_3,t_4)$.

1. The knot vector for uniform bsplines curve requires the following conditions: $t_{j+1} = t_j + k$
   where k is any constant scalar value.
   Example: $n = 2$ and $d = 2$ then $k = 1$, $\mathbf{t} = (t_0,t_1,t_2,t_3,t_4) = (0,1,2,3,4)$
   In open uniform, multiplicity of knot values at ends are equal to the order of the Bspline curve and internal knot values are evenly spaced.

2. The knot vector for non-uniform bsplines curve requires the following general condition: $t_{j+1} \geq t_j$
   One of the forms of non-uniform knot vector is as follows:

$$\begin{cases} t_j = 0 & \text{if } j < d \\ t_j = j - d + 1 & \text{if } d \leq j \leq d \\ t_j = n - d + 2 & \text{if } j > n \end{cases} \tag{3.5}$$

   Example:$n = 2$ and $d = 2$ produces $\mathbf{t} = (t_0,t_1,t_2,t_3,t_4)$=(0,0,1,2,2)

In this thesis, uniform knot vectors are used to calculate B-spline curves and basis functions. The figures shown below illustrates bspline basis function having uniform knot spaces for linear, quadratic and cubic polynomial approximation.

There are some more important points about B-Splines that are worth mentioning:

1. Convex hull property: the curve is contained inside the convex hull of the control polygon.
2. The control points are not interpolated, in general.
3. Affine transformations of the B-Spline curve are performed by transforming the control points correspondingly.
4. The control points have influence on maximum p + 1 sections, allowing local control.

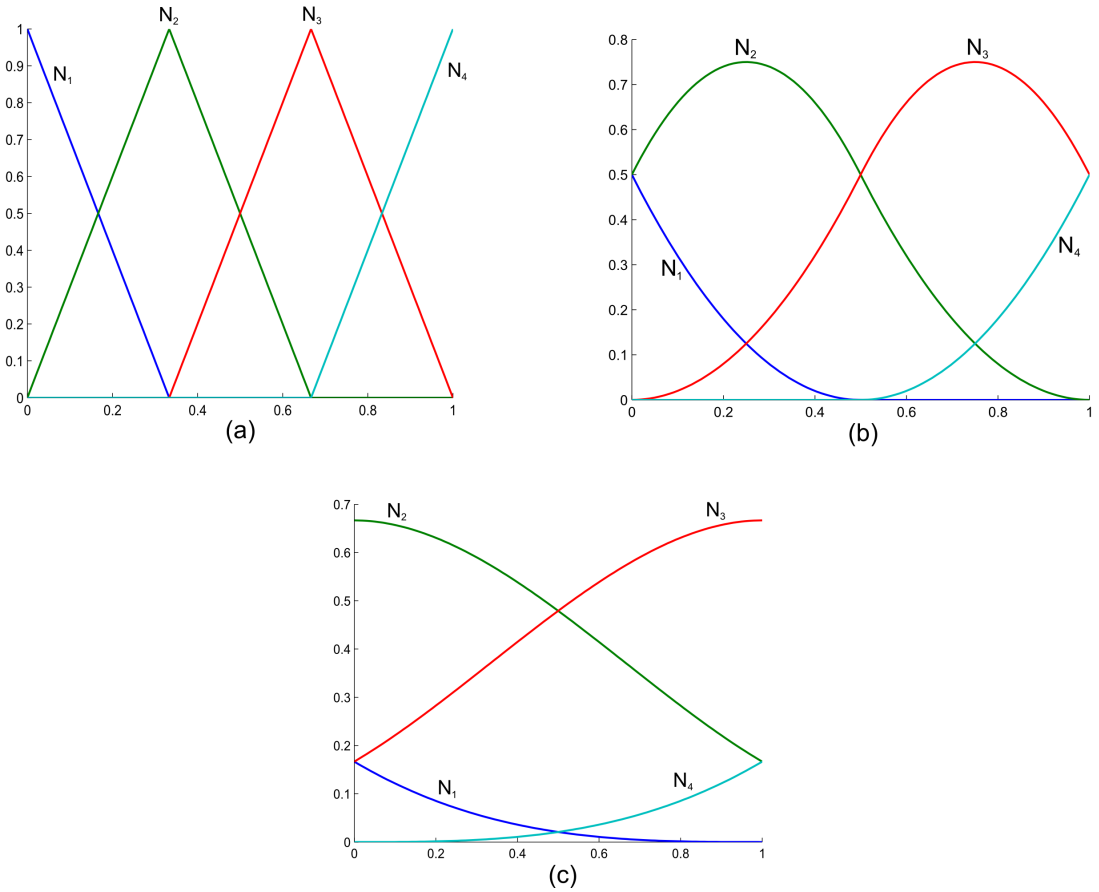

Figure 3.1: Uniform B-Spline Basis Functions (a)Linear (b)Quadratic (c)Cubic

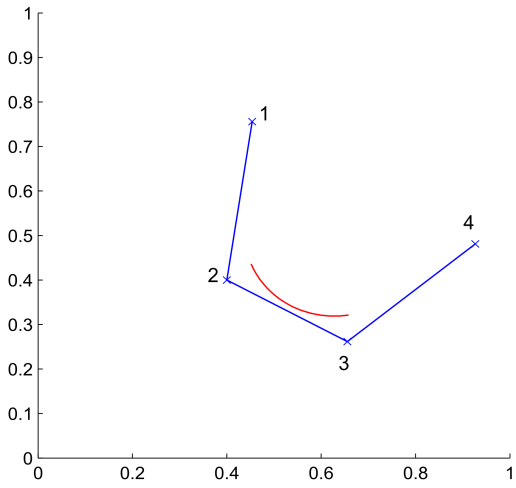

Figure 3.2: Function interpolation with Uniform Cubic B-Splines

4

Finite Element Discretization of a Beam with B-Spline Shape Functions

In this section, the beam equations are derived from the weak form of virtual work principle and then discretized using B-Spline shape functions. Here, it is assumed that the centerline of the beam is embedded in the two dimensional space and thus the discretization is needed to be done only over the centerline. Further, the terms for internal force and tangent stiffness matrix are derived which are needed for nonlinear analysis of the beam. All the governing equations are formulated in a similar fashion as done by (Cirak et al. 2000) used for subdivision shell, with assumptions valid for Euler-Bernoulli beam. The advantage of doing so, is its easy extension to thin shell model.

4.1 Kinematics of a beam embedded in 2D

A beam is considered whose undeformed geometry $\bar{\mathcal{B}}$ is characterized by a centerline ($\overline{\Omega}$). The beam deforms in the action of applied loads and adopts a deformed configuration characterized by a deformed center line(Ω). The position vector of material point $\bar{\mathbf{r}} \in \mathcal{B}_o$ in the reference and $\mathbf{r} \in \mathcal{B}_t$ in the deformed configurations of the beam body may be parametrized in terms of arc-length $\theta^1 \in \omega \subset \mathbb{R}$ and the two coordinates $\theta^2 \in [-h/2,h/2]$ and $\theta^3 \in [-b/2,b/2]$.The later coordinates are orthogonal to the centre line and span the beam height h and depth b.

$$\bar{\mathbf{r}}(\theta^1,\theta^2,\theta^3) = \overline{\mathbf{x}}(\theta^1) + \theta^2\overline{\mathbf{a}_2}(\theta^1) + \theta^3\overline{\mathbf{a}_3} \tag{4.1}$$

$$\mathbf{r}(\theta^1,\theta^2,\theta^3) = \mathbf{x}(\theta^1) + \theta^2\mathbf{a}_2(\theta^1) + \theta^3\mathbf{a}_3 \tag{4.2}$$

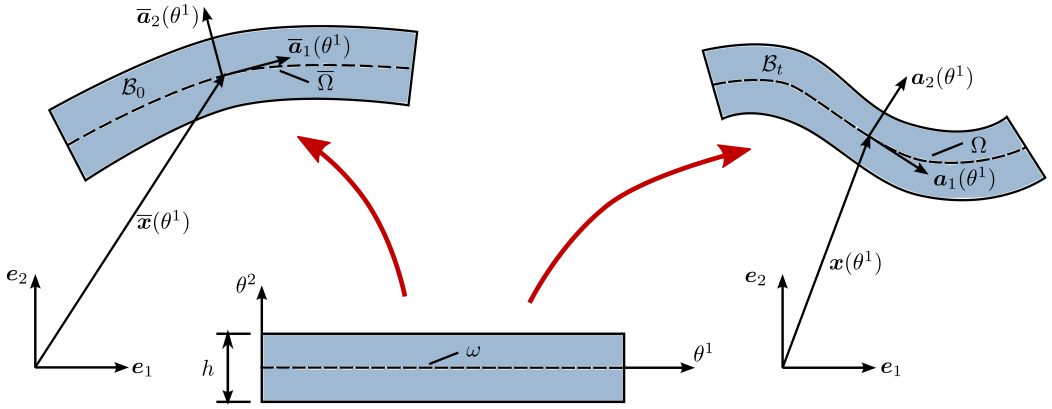

Figure 4.1: Beam in the reference (left) and deformed (right) configurations

where $\overline{\mathbf{x}}$ and $\mathbf{x}$ are the undeformed and deformed center line position vector of the beam. The unit vectors $\overline{\mathbf{a}}_2$, $\mathbf{a}_2$ and $\overline{\mathbf{a}}_3$, $\mathbf{a}_3$ are orthogonal to the tangent of the center line, c.f. Figure 4.1. The tangent vectors to the curve in the reference and deformed configurations are:

$$\overline{\mathbf{a}}_1 = \frac{\mathrm{d}\overline{\mathbf{x}}}{\mathrm{d}\theta^1} = \overline{\mathbf{x}}' \tag{4.3}$$

$$\mathbf{a}_1 = \frac{\mathrm{d}\mathbf{x}}{\mathrm{d}\theta^1} = \mathbf{x}' \tag{4.4}$$

In the following it is assumed that only one dimensional beam centre line is embedded in a two dimensional space. Therefore, the binormal $\overline{\mathbf{a}}_3 = \mathbf{a}_3 = \mathbf{e}_3$ may be considered as the unit vector normal to the embedding space. Hence, the unit normal to the centre line in the reference and deformed configurations are:

$$\overline{\mathbf{a}}_2 = \overline{\mathbf{a}}_3 \times \frac{\overline{\mathbf{a}}_1}{|\overline{\mathbf{a}}_1|} \tag{4.5}$$

$$\mathbf{a}_2 = \mathbf{a}_3 \times \frac{\mathbf{a}_1}{|\mathbf{a}_1|} \tag{4.6}$$

Their derivative with respect to longitudinal parameter θ^1 are:

$$\overline{\mathbf{a}}_2' = \overline{\mathbf{a}}_3 \times \frac{\overline{\mathbf{a}}_1'}{|\overline{\mathbf{a}}_1|} - \frac{\overline{\mathbf{a}}_1 \cdot \overline{\mathbf{a}}_1'}{|\overline{\mathbf{a}}_1|^2}\overline{\mathbf{a}}_2 \tag{4.7}$$

$$\mathbf{a}_2' = \mathbf{a}_3 \times \frac{\mathbf{a}_1'}{|\mathbf{a}_1|} - \frac{\mathbf{a}_1 \cdot \mathbf{a}'_1}{|\mathbf{a}_1|^2}\mathbf{a}_2 \tag{4.8}$$

The covariant basevectors, i.e tangent vectors of the beam body follow from:

$$\overline{\mathbf{g}}_\alpha = \frac{\mathrm{d}\overline{\mathbf{r}}}{\mathrm{d}\theta^\alpha} \qquad \text{with} \qquad \overline{\mathbf{g}}_1 = \frac{\mathrm{d}\overline{\mathbf{r}}}{\mathrm{d}\theta^1} = \overline{\mathbf{x}}' + \theta^2\overline{\mathbf{a}}_2' = \overline{\mathbf{a}}_1 + \theta^2\overline{\mathbf{a}}_2' \tag{4.9}$$

$$\mathbf{g}_\alpha = \frac{\mathrm{d}\mathbf{r}}{\mathrm{d}\theta^\alpha} \qquad \text{with} \qquad \mathbf{g}_1 = \frac{\mathrm{d}\mathbf{r}}{\mathrm{d}\theta^1} = \mathbf{x}' + \theta^2\mathbf{a}_2' = \mathbf{a}_1 + \theta^2\mathbf{a}_2' \tag{4.10}$$

and the matrix of the co- and contra-variant metrics is defined by:

$$[\overline{g}_{\alpha\beta}] = [\overline{\mathbf{g}}_\alpha \cdot \overline{\mathbf{g}}_\beta] = \begin{bmatrix} \overline{g}_{11} & 0 & 0 \\ 0 & 1 & 0 \\ 0 & 0 & 1 \end{bmatrix} \quad \text{and} \quad [\overline{g}^{\alpha\beta}] = [\overline{g}_{\alpha\beta}]^{-1} = \begin{bmatrix} 1/\overline{g}_{11} & 0 & 0 \\ 0 & 1 & 0 \\ 0 & 0 & 1 \end{bmatrix} \tag{4.11}$$

By restricting the beam motion to the aformentioned model a diagonal matrix is obtained in which only the 11-entry can be a non-unit entry. This entry is in particular:

$$\overline{g}_{11} = \overline{\mathbf{g}}_1 \cdot \overline{\mathbf{g}}_1 \quad \text{and} \quad g_{11} = \mathbf{g}_1 \cdot \mathbf{g}_1 \tag{4.12}$$

Using these expressions the Green–Lagrange axial strain of the beam, i.e. $E_{11} = \frac{1}{2}(g_{11} - \overline{g}_{11})$, is found to be:

$$E_{11} = \frac{1}{2}\left(\mathbf{a}_1 \cdot \mathbf{a}_1 - \overline{\mathbf{a}}_1 \cdot \overline{\mathbf{a}}_1\right) - \theta^2 \left(\mathbf{a}_2 \cdot \mathbf{a}_1' - \overline{\mathbf{a}}_2 \cdot \overline{\mathbf{a}}'_1\right) \tag{4.13}$$

whereby the relation $\mathbf{a}_1 \cdot \mathbf{a}_2' = -\mathbf{a}_1' \cdot \mathbf{a}_2$ is used. The latter can be deduced from their orthogonality $\mathbf{a}_1 \cdot \mathbf{a}_2 = 0$ and thus $(\mathbf{a}_1 \cdot \mathbf{a}_2)' = \mathbf{a}_1' \cdot \mathbf{a}_2 + \mathbf{a}_1 \cdot \mathbf{a}_2' = 0$. The quadratic terms in θ^2 have been neglected. The first term in E_{11} is related to the membrane straining and the second term to the beam curvature change. Thus what follows is:

$$\begin{aligned} E_{11} = \alpha + \theta^2 \beta \quad \text{with} \quad \alpha &= \frac{1}{2}\left(\mathbf{a}_1 \cdot \mathbf{a}_1 - \overline{\mathbf{a}}_1 \cdot \overline{\mathbf{a}}_1\right), \\ \beta &= -\left(\mathbf{a}_2 \cdot \mathbf{a}_1' - \overline{\mathbf{a}}_2 \cdot \overline{\mathbf{a}'}_1\right). \end{aligned} \tag{4.14}$$

Here, the curvature of the curve is defined by $\mathbf{a}_2 \cdot \mathbf{a}_1'$.

4.2 Weak form of governing equations

The weak form of balance of momentum in the reference configuration is given as:

$$\begin{cases} \underbrace{\int\limits_{\overline{\mathcal{B}}} \mathbf{S} : \delta\mathbf{E} \, \mathrm{d}V}_{\delta\pi_{int}} = \underbrace{\int\limits_{\overline{\mathcal{B}}} \hat{\mathbf{b}}_0 \cdot \delta\mathbf{r} \, \mathrm{d}V + \int\limits_{\partial_{\mathrm{N}}\overline{\mathcal{B}}} \hat{\mathbf{t}}_0 \cdot \delta\mathbf{r} \, \mathrm{d}A}_{\delta\pi_{ext}} + \int\limits_{\partial_{\mathrm{N}}\overline{\mathcal{B}}} \boldsymbol{\lambda} \cdot \delta\mathbf{r} \, \mathrm{d}V \\ \int\limits_{\partial_D\overline{\mathcal{B}}} (\mathbf{r} - \hat{\mathbf{r}}) \cdot \delta\boldsymbol{\lambda} \, \mathrm{d}V = 0 \end{cases} \tag{4.15}$$

Here, the so-called generalised weak form is used to incorporate weak satisfaction of the Dirichlet boundary conditions. The Lagrange multiplier $\boldsymbol{\lambda}$ is a traction field on the Dirichlet boundary. The 2nd Piola–Kirchhoff stress $\mathbf{S}$ is related to the Green–Lagrange

strain $\mathbf{E}$ with the hyperelastic potential energy density W:

$$\mathbf{S} = \frac{\partial W}{\partial \mathbf{E}} \tag{4.16}$$

The volume integration is carried out on the convected parameters $(\theta^1, \theta^2, \theta^3)$ which gives

$$\int_{\overline{\mathcal{B}}} (\bullet)\, \mathrm{d}\, V = \int_b \int_h \int_\omega (\bullet)\, \sqrt{\overline{g}} \mathrm{d}\theta^1 \mathrm{d}\theta^2 \mathrm{d}\theta^3 \tag{4.17}$$

The jacobian determinant is determined as follows:

$$\begin{aligned} \sqrt{\overline{g}} = \det[\overline{\mathbf{g}}_1\ \overline{\mathbf{g}}_2\ \overline{\mathbf{g}}_3] = \overline{\mathbf{g}}_1 \cdot (\overline{\mathbf{g}}_3 \times \overline{\mathbf{g}}_3) = (\overline{\mathbf{a}}_1 + \theta^2 \overline{\mathbf{a}}_2') \cdot (\overline{\mathbf{a}}_2 \times \overline{\mathbf{a}}_3) \\ = (\overline{\mathbf{a}}_1 + \theta^2 \overline{\mathbf{a}}_2') \cdot \frac{\overline{\mathbf{a}}_1}{|\mathbf{a}_1|} = \overline{\mathbf{a}}_1 + \theta^2 \frac{\overline{\mathbf{a}}_2' \cdot \overline{\mathbf{a}}_1}{|\overline{\mathbf{a}}_1|} \end{aligned} \tag{4.18}$$

after introducing (4.5) and (4.7). Alternatively, the Jacobian determinant can be derived using the contra-variant metric coefficients, i.e.

$$\overline{g} = \det[\overline{\mathbf{g}}_{\alpha\beta}] = \overline{g}_{11} = |\overline{\mathbf{a}}_1|^2 + 2\theta^2 \overline{\mathbf{a}}_1 \cdot \overline{\mathbf{a}}_2' + (\theta^2)^2 \left(\frac{\overline{\mathbf{a}}_2' \cdot \overline{\mathbf{a}}_2'}{|\overline{\mathbf{a}}_1|} \right)^2 \tag{4.19}$$

This form is equivalent, as expected, after realising that the derivative of the normal base vector is a vector in tangent direction, i.e. $\overline{\mathbf{a}}_2' = b_2^1 \overline{\mathbf{a}}_1$.
We can use the metric $\overline{g}$ to express the current infinitesimal arc-length $\mathrm{d}\Omega$ as:

$$\mathrm{d}\Omega = \sqrt{\overline{g}} \mathrm{d}\theta^1 = \underbrace{\left(1 - \theta^2 \underbrace{\frac{\overline{\mathbf{a}}_1' \cdot \overline{\mathbf{a}}_2}{\overline{\mathbf{a}}_1 \cdot \overline{\mathbf{a}}_1}}_{\overline{\eta}} \right)}_{\overline{\mu}} \underbrace{|\overline{\mathbf{a}}_1| \mathrm{d}\theta^1}_{\mathrm{d}\overline{\Omega}} = \overline{\mu}\, \mathrm{d}\overline{\Omega} \tag{4.20}$$

The scalar $\overline{\mu}(\theta^1,\theta^2) = 1 - \theta^2 \overline{\eta}(\theta^1)$ contains the change of the metric on the beam surface with respect to the initial, curvilinear, convected parameters. In case of an initially straight beam the factor $\overline{\eta}$ is zero. With $\overline{\mu}$ the volume integral is expressed as:

$$\int_{\overline{\mathcal{B}}} (\bullet)\ \mathrm{d}\, V = \int_b \int_h \int_\omega (\bullet)\, \overline{\mu} \mathrm{d}\overline{\Omega} \mathrm{d}\theta^2 \mathrm{d}\theta^3 \tag{4.21}$$

4.2.1 End-point external traction

A linear traction is applied on the boundary Γ of the beam. The beam model is for thin beams such that the height h remains unchanged during deformation. This fact can be also deduced from the Jacobian $\overline{\mu}$. Consequently, the Cauchy and Piola boundary

traction are equal, i.e. $\hat{\mathbf{t}}_0 = \frac{\mathrm{d}A}{\mathrm{d}\overline{A}}\hat{\mathbf{t}} = \hat{\mathbf{t}}$ We define a Cauchy traction as:

$$\hat{\mathbf{t}} = \hat{s}^1\mathbf{e}_1 + \hat{s}^2\mathbf{e}_2 - \theta^2\hat{q}\mathbf{n} \quad \text{with} \quad \mathbf{n} = \frac{\mathbf{a}_1}{|\mathbf{a}_1|} \quad \text{and} \quad \hat{s}^1, \hat{s}^2, \hat{q} = \text{const} \tag{4.22}$$

on Γ. The first term will result in a force in $\mathbf{e}_1$-direction. The second likewise determines a force in $\mathbf{e}_2$-direction. The third term defines a follower force couple equivalent to a torque around the $\mathbf{e}_3$ axis. Later on, we discretise the beam with a pure displacement-based formulation in which rotational degrees-of-freedom do not occur. Thus, the end-point torque is indeed modelled with a couple of consistent follower forces.

The outward unit normal $\mathbf{n}$ on the boundary in the deformed configuration is expressed in terms of the tangent $\mathbf{a}_1$ to the centre line due to the thin beam model.

In case an end-point axial and shear force is sought, the Cartesian base vectors $\mathbf{e}_1$ and $\mathbf{e}_2$ in (4.23) must be replaced by $\mathbf{n}$ and $\mathbf{a}_2$, respectively. These are also follower load.

The equivalent Piola traction $\hat{\mathbf{t}}_0 = \hat{\mathbf{t}}$ is introduced in the external virtual work expression yielding

$$\begin{aligned}
\int_{\overline{\Gamma}} \hat{\mathbf{t}_0} \cdot \delta\mathbf{r}\mathrm{d}A &= \int_b \int_h \left(\hat{s}^1\mathbf{e}_1 + \hat{s}^2\mathbf{e}_2 - \theta^2\hat{q}\mathbf{n}\right) \cdot \left(\delta\mathbf{x} + \theta^2\delta\mathbf{a}_2\right)\Big|_{\theta^1=\partial\omega} \mathrm{d}\theta^2\mathrm{d}\theta^3 \\
&= \left(\underbrace{bh\hat{s}^1}_{\hat{P}^1}\mathbf{e}_1 \cdot \delta\mathbf{x} + \underbrace{bh\hat{s}^2}_{\hat{P}^2}\mathbf{e}_2 \cdot \delta\mathbf{x} - \underbrace{\frac{bh^3}{12}\hat{q}}_{\hat{M}}\mathbf{n} \cdot \delta\mathbf{a}_2\right)\Bigg|_{\theta^1=\partial\omega}
\end{aligned} \tag{4.23}$$

The following shear resulants occur: normal force $\hat{P}^1$, shear force $\hat{P}^2$ and torque $\hat{M}$. We take the orthogonality of $\mathbf{n}$ and $\mathbf{a}_2$ into account, i.e. $\mathbf{n} \cdot \delta\mathbf{a}_2 = -\mathbf{a}_2 \cdot \delta\mathbf{n}$. Using the orthogonality relation, the virtual external works simplifies to:

$$\int_{\overline{\Gamma}} \hat{\mathbf{t}_0} \cdot \delta\mathbf{r}\mathrm{d}A = \left(\hat{P} \cdot \delta\mathbf{x} + \hat{M}\underbrace{\mathbf{a}_2 \cdot \frac{\delta\mathbf{a}_1}{|\mathbf{a}_1|}}_{\delta\phi}\right)\Bigg|_{\theta^1=\partial\omega} \tag{4.24}$$

$\mathbf{a}_2 \cdot \frac{\delta\mathbf{a}_1}{|\mathbf{a}_1|}$ is actually the virtual rotation $\delta\phi$ around the $\mathbf{e}_3$-axis. Similarly, the body load density is given by:

$$\hat{b} = \hat{s}^1\mathbf{e}_1 + \hat{s}^2\mathbf{e}_2 - \theta^2\hat{q}\frac{\mathbf{a}_1}{|\mathbf{a}_1|} \tag{4.25}$$

leads to

$$\begin{aligned}
\int_{\overline{\mathcal{B}}} \hat{\mathbf{b}_0} \cdot \delta\mathbf{r}\mathrm{d}\,V = \int_{\overline{\Omega}} \Bigg(&\underbrace{(A - \overline{\eta}I)\hat{s}^1}_{\overline{p}^1}\mathbf{e}_1 \cdot \delta\mathbf{x} + \quad \underbrace{(A - \overline{\eta}I)\hat{s}^2}_{\overline{p}^2}\mathbf{e}_2 \cdot \delta\mathbf{x} - \\
&\underbrace{(1 - \overline{\eta})I\hat{q}}_{\overline{m}}\frac{\mathbf{a}_1}{|\mathbf{a}_1|} \cdot \delta\mathbf{a}_2\Bigg)\mathrm{d}\overline{\Omega}
\end{aligned} \tag{4.26}$$

with cross section area $A = bh$ and 2nd moment of area $I = bh^3/12$. Finally, we denote it by:

$$\int_{\overline{\mathcal{B}}} \hat{\mathbf{b}_0} \cdot \delta\mathbf{r} \mathrm{d}\, V = \int_{\overline{\Omega}} \left(\hat{\mathbf{p}} \cdot \delta\mathbf{x} + \hat{m}_2 \cdot \underbrace{\frac{\delta\mathbf{a}_1}{|\mathbf{a}_1|}}_{\delta\phi} \right) \mathrm{d}\overline{\Omega} \tag{4.27}$$

with the distributed forces $\hat{\mathbf{p}}$ (force per length) and torque $\hat{m}$ (moment per length)

4.3 Discretized Beam Governing Equations

The domain $\mathrm{d}\overline{\Omega}$ is discretised with NEL elements. The volume integrals are approximated with the sum over the sub-integrals on the element domains. Moreover, the position of the centre line is discretised with NNP shape functions $N^K(\theta^1)$ and nodal position vectors $\overline{\mathbf{x}}_K$ and $\mathbf{x}_K$ in reference and current configuration, respectively:

$$\overline{\mathbf{x}}(\theta^1,t) = \sum_{K=1}^{NNP} \mathbf{N}^K(\theta^1)\overline{\mathbf{x}}_K \tag{4.28}$$

$$\mathbf{x}(\theta^1,t) = \sum_{K=1}^{NNP} \mathbf{N}^K(\theta^1)\mathbf{x}_K \tag{4.29}$$

Note, the shape functions $N^K(\theta^1)$ are defined on the dimensionless convected parametric coordinate $\theta^1 \in \omega$ co-ordinate.

4.3.1 Internal Forces

Next the interpolation is introduced into the internal virtual work equation(4.15) and the nodal internal forces follow from:

$$\delta\pi_{int} = \mathbf{f}^K_{int} \cdot \delta\mathbf{x}_K = \int_{\overline{\mathcal{B}}} \mathbf{S} : \frac{\partial \mathbf{E}}{\partial \mathbf{x}_K} \mathrm{d}\, V \cdot \delta\mathbf{x}_K \tag{4.30}$$

Next, we consider the Green–Lagrange strain and 2nd Piola–Kirchhoff stress components in convected co-ordinates, i.e.

$$\mathbf{E} = E_{\alpha\beta}\overline{\mathbf{g}}^\alpha \otimes \overline{\mathbf{g}}^\beta \quad \text{and} \quad \mathbf{S} = S^{\alpha\beta}\overline{\mathbf{g}}_\alpha \otimes \overline{\mathbf{g}}_\beta \tag{4.31}$$

By assumption, except S^{11} all the stress components are zero. This implies

$$\mathbf{f}^K_{int} = \int_{\overline{\Omega}} \int_h \int_b S^{11} \frac{\partial E^{11}}{\partial \mathbf{x}_K} \overline{\mu} \mathrm{d}\theta^3 \mathrm{d}\theta^2 \mathrm{d}\overline{\Omega} \tag{4.32}$$

As the strains are assumed to be small, St.Venant–Kirchhoff constitutive equation can be used:

$$S^{11} = C^{1111} E_{11} \quad \text{with} \quad C^{1111} = E\overline{g}^{11}\overline{g}^{11} = \frac{E}{\overline{g}_{11}\overline{g}_{11}} =: C \tag{4.33}$$

where E is Young's modulus and $\overline{g}^{11}$ is the 11-entry of the contra-variant metric coefficients. Note, $\overline{g}^{11}$ depends in general on θ^1 and θ^2. The linear material relation is introduced in the internal forces and gives:

$$\begin{aligned}
\mathbf{f}^K_{int} &= \int_{\overline{\Omega}} \int_h \int_b E^{11} C \frac{\partial E^{11}}{\partial \mathbf{x}_K} \overline{\mu} \mathrm{d}\theta^3 \mathrm{d}\theta^2 \mathrm{d}\overline{\Omega} \\
&= \int_{\overline{\Omega}} \int_h \int_b (\alpha + \theta^2 \beta) C (\frac{\partial \alpha}{\partial \mathbf{x}_K} + \theta^2 \frac{\partial \beta}{\partial \mathbf{x}_K}) \overline{\mu} \mathrm{d}\theta^3 \mathrm{d}\theta^2 \mathrm{d}\overline{\Omega} \\
&= \int_{\overline{\Omega}} \int_h \int_b \left(\alpha C \frac{\partial \alpha}{\partial \mathbf{x}_K} + \theta^2 (\beta C \frac{\partial \alpha}{\partial \mathbf{x}_K} + \alpha C \frac{\partial \beta}{\partial \mathbf{x}_K}) + (\theta^2)^2 \beta C \frac{\partial \beta}{\partial \mathbf{x}_K} \right) \overline{\mu} \mathrm{d}\theta^3 \mathrm{d}\theta^2 \mathrm{d}\overline{\Omega}
\end{aligned} \tag{4.34}$$

Note that the integrals over the cross section can be evaluated analytically, which leads to

$$\mathbf{f}^K_{int} = \int_{\overline{\Omega}} \left(CA\alpha \frac{\partial \alpha}{\partial \mathbf{x}_K} + CI\beta \frac{\partial \beta}{\partial \mathbf{x}_K} \right) \mathrm{d}\overline{\Omega} + \int_{\overline{\Omega}} \left(CI\beta \frac{\partial \alpha}{\partial \mathbf{x}_K} + CI\alpha \frac{\partial \beta}{\partial \mathbf{x}_K} \right) \mathrm{d}\overline{\Omega} \tag{4.35}$$

where $A = bh$ is the area of the cross section and $I = \frac{1}{12} bh^3$ is the moment of inertia of the cross section. The second integral is neglected, it is only present in initially curved beams. Further, the membrane force is defined as $n = CA\alpha$ and the couple force as $m = CA\beta$. Introducing these notations the internal forces become:

$$\mathbf{f}^K_{int} = \int_{\overline{\Omega}} (n \frac{\partial \alpha}{\partial \mathbf{x}_K} + m \frac{\partial \beta}{\partial \mathbf{x}_K}) \mathrm{d}\overline{\Omega} \tag{4.36}$$

The derivatives of the strain type variables with respect to the deformed nodal positions are:

$$\frac{\partial \alpha}{\partial \mathbf{x}_K} = \mathbf{a}_1 \cdot \frac{\partial \mathbf{a}_1}{\partial \mathbf{x}_K} \tag{4.37}$$

$$\frac{\partial \beta}{\partial \mathbf{x}_K} = -\frac{\partial \mathbf{a}_2}{\partial \mathbf{x}_K} \cdot \mathbf{a}_1' - \mathbf{a}_2 \cdot \frac{\partial \mathbf{a}_1'}{\partial \mathbf{x}_K} \tag{4.38}$$

The variation of the tangent vector yields to:

$$\frac{\partial \mathbf{a}_1}{\partial \mathbf{x}_K} = N'^J \frac{\partial \mathbf{x}_J}{\partial \mathbf{x}_K} = N'^J \mathbf{I} \quad \text{or} \quad \frac{\partial a^i_1}{\partial x^j_K} = N'^J \frac{\partial x^i_J}{\partial x^j_K} = N'^K \delta^i_j \tag{4.39}$$

and the normal vector result in

$$\frac{\partial \mathbf{a}_2}{\partial \mathbf{x}_K} = \frac{1}{|\mathbf{a}_1|}\mathbf{a}_3 \times \frac{\partial \mathbf{a}_1}{\partial \mathbf{x}_K} - \mathbf{a}_2 \left(\frac{\mathbf{a}_1}{|\mathbf{a}_1|^2} \cdot \frac{\partial \mathbf{a}_1}{\partial \mathbf{x}_K} \right) \tag{4.40}$$

The variation of the derived tangent vector is straight forward

$$\frac{\partial \mathbf{a}_1'}{\partial \mathbf{x}_K} = N''^J \frac{\partial \mathbf{x}_J}{\partial \mathbf{x}_K} = N''^J \mathbf{I} \quad \text{or} \quad \frac{\partial a_1^i}{\partial x_K^j} = N''^J \frac{\partial x_J^i}{\partial x_K^j} = N''^K \delta_j^i \tag{4.41}$$

4.3.2 Stiffness matrix of internal forces

The nodal Hessian of the potential energy is:

$$\mathbf{k}_{int}^{KJ} = \frac{\partial \mathbf{f}_{int}^K}{\partial \mathbf{x}_K} = \int_{\overline{\Omega}} \left(\frac{\partial n}{\partial \mathbf{x}_L} \frac{\partial \alpha}{\partial \mathbf{x}_K} + n \frac{\partial^2 \alpha}{\partial \mathbf{x}_K \partial \mathbf{x}_L} + \frac{\partial m}{\partial \mathbf{x}_K} \frac{\partial \beta}{\partial \mathbf{x}_K} + m \frac{\partial^2 \beta}{\partial \mathbf{x}_K \partial \mathbf{x}_L} \right) \mathrm{d}\overline{\Omega} \tag{4.42}$$

The second derivatives of the strain type variables with respect to the deformed nodal positions are:

$$\frac{\partial^2 \alpha}{\partial \mathbf{x}_K \partial \mathbf{x}_L} = \frac{\partial}{\partial \mathbf{x}_L} \left(\mathbf{a}_1 \cdot \frac{\partial \mathbf{a}_1}{\partial \mathbf{x}_K} \right) = \frac{\partial \mathbf{a}_1}{\partial \mathbf{x}_L} \cdot \frac{\partial \mathbf{a}_1}{\partial \mathbf{x}_K} + \mathbf{a}_1 \cdot \frac{\partial^2 \mathbf{a}_1}{\partial \mathbf{x}_K \partial \mathbf{x}_L} \tag{4.43}$$

$$\frac{\partial^2 \beta}{\partial \mathbf{x}_K \partial \mathbf{x}_L} = -\frac{\partial^2 \mathbf{a}_2}{\partial \mathbf{x}_K \partial \mathbf{x}_L} \cdot \mathbf{a}_1' - \frac{\partial \mathbf{a}_2}{\partial \mathbf{x}_K} \cdot \frac{\partial \mathbf{a}_1'}{\partial \mathbf{x}_L} - \frac{\partial \mathbf{a}_2}{\partial \mathbf{x}_L} \cdot \frac{\partial \mathbf{a}_1'}{\partial \mathbf{x}_K} - \mathbf{a}_2 \cdot \frac{\partial^2 \mathbf{a}_1'}{\partial \mathbf{x}_K \partial \mathbf{x}_L} \tag{4.44}$$

The second derivative of the normal director is:

$$\begin{aligned} \frac{\partial^2 \mathbf{a}_2}{\partial \mathbf{x}_K \partial \mathbf{x}_L} = &- \left(\frac{\partial \mathbf{a}_1}{|\mathbf{a}_1|^3} \cdot \frac{\partial a_1}{\partial \mathbf{x}_L} \right) \left(\mathbf{a}_3 \times \frac{\partial \mathbf{a}_1}{\partial \mathbf{x}_K} \right) - \left(\frac{\mathbf{a}_1}{|\mathbf{a}_1|^2} \cdot \frac{\partial \mathbf{a}_1}{\partial \mathbf{x}_K} \right) \frac{\partial \mathbf{a}_2}{\partial \mathbf{x}_L} \\ &- \frac{1}{|\mathbf{a}_1|^2} \left(\frac{\partial \mathbf{a}_1}{\partial \mathbf{x}_L} \cdot \frac{\partial \mathbf{a}_1}{\partial \mathbf{x}_K} \right) \mathbf{a}_2 + \frac{1}{|\mathbf{a}_1|^4} \left(\mathbf{a}_1 \cdot \frac{\partial \mathbf{a}_1}{\partial \mathbf{x}_L} \right) \left(\mathbf{a}_1 \cdot \frac{\partial \mathbf{a}_1}{\partial \mathbf{x}_K} \right) \mathbf{a}_2 \end{aligned} \tag{4.45}$$

4.3.3 External forces

The external forces result from the virtual external work after introducing the approximation approach:

$$\delta \pi_{ext} = \mathbf{f}_{ext}^K \cdot \delta \mathbf{x}_K = \left(\int_{\overline{\mathcal{B}}} \hat{\mathbf{b}_0} \cdot \frac{\partial \mathbf{r}}{\partial \mathbf{x}_K} \mathrm{d}\, V + \int_{\partial_{\mathrm{N}} \overline{\mathcal{B}}} \hat{\mathbf{t}_0} \cdot \frac{\partial \mathbf{r}}{\partial \mathbf{x}_K} \mathrm{d}A \right) \cdot \delta \mathbf{x}_K \tag{4.46}$$

Only linear body loads $\hat{\mathbf{b}_0} = \text{const}$ and the end-point loads are considered as described in Section 4.2.1. The work integral simplifies to

$$\mathbf{f}_{ext}^{K} = \int_{\overline{\Omega}} \left(\hat{\mathbf{p}} \cdot \frac{\partial \mathbf{x}}{\partial \mathbf{x}_K} + \hat{m} \frac{\mathbf{a}_2}{|\mathbf{a}_1|} \cdot \frac{\partial \mathbf{a}_1}{\partial \mathbf{x}_K} \right) \mathrm{d}\overline{\Omega} + \left(\hat{\mathbf{P}} \cdot \frac{\partial \mathbf{x}}{\partial \mathbf{x}_K} + \hat{M} \frac{\mathbf{a}_2}{|\mathbf{a}_1|} \cdot \frac{\partial \mathbf{a}_1}{\partial \mathbf{x}_K} \right) \Bigg|_{\theta^1 = \partial\omega} \tag{4.47}$$

4.3.4 Stiffness Matrix of External Forces

The moments are consistently discretised as follower force couples. Therefore, the tangent of these forces with respect to the current node positions does not vanish. The following external stiffness matrix emerges

$$\mathbf{k}_{ext}^{KJ} = \frac{\partial \mathbf{f}_{ext}^{K}}{\partial \mathbf{x}_K} = \int_{\overline{\Omega}} \hat{m} \frac{\partial}{\partial \mathbf{x}_L} \left(\frac{\mathbf{a}_2}{|\mathbf{a}_1|} \cdot \frac{\partial \mathbf{a}_1}{\partial \mathbf{x}_K} \right) \mathrm{d}\overline{\Omega} + \hat{M} \frac{\partial}{\partial \mathbf{x}_L} \left(\frac{\mathbf{a}_2}{|\mathbf{a}_1|} \cdot \frac{\partial \mathbf{a}_1}{\partial \mathbf{x}_K} \right) \Bigg|_{\theta^1 = \partial\omega} \tag{4.48}$$

with

$$\frac{\partial}{\partial \mathbf{x}_L} \left(\frac{\mathbf{a}_2}{|\mathbf{a}_1|} \cdot \frac{\partial \mathbf{a}_1}{\partial \mathbf{x}_K} \right) = \frac{1}{|\mathbf{a}_1|} \frac{\partial \mathbf{a}_2}{\partial \mathbf{x}_L} \cdot \frac{\partial \mathbf{a}_1}{\partial \mathbf{x}_K} - \left(\frac{\mathbf{a}_1}{|\mathbf{a}_1|^3} \cdot \frac{\partial \mathbf{a}_1}{\partial \mathbf{x}_L} \right) \left(\mathbf{a}_2 \cdot \frac{\partial \mathbf{a}_1}{\partial \mathbf{x}_K} \right) \tag{4.49}$$

4.4 Finite Element Approximation with B-Spline Shape Functions

For the parametrization of the curve the usual B-spline shape functions are used. A uniform bspline is a composite of cubic Bezier curve segments as discussed in Chapter 3. Each element has a parametric domain ω^e which are a partition of the beam domain $\omega = \bigcup_e \omega^e$. The shape functions on one finite element are controlled by four control points. The uniform B-Spline shape functions are described over the dimensionless parameter $\xi = [0, 1]$ one each element

$$N^1(\xi) = \frac{1}{6}(-\xi^3 + 3\xi^2 - 3\xi + 1) \tag{4.50}$$

$$N^2(\xi) = \frac{1}{6}(3\xi^3 - 6\xi^2 + 4) \tag{4.51}$$

$$N^3(\xi) = \frac{1}{6}(-3\xi^3 + 3\xi^2 + 3\xi + 1) \tag{4.52}$$

$$N^4(\xi) = \frac{1}{6}(\xi^3) \tag{4.53}$$

Boundary Condition	$u(x)\|_{x=0 \text{ or } l}$	$u'(x)\|_{x=0 \text{ or } l}$	$u''(x)\|_{x=0 \text{ or } l}$	$u'''(x)\|_{x=0 \text{ or } l}$
Clamped	0	0		
Pinned	0		0	
Free			0	0
Guided		0		0

Table 4.1: Boundary Conditions of the Beam

Using similar approach as in section 4.3, it can be written as:

$$\overline{\mathbf{x}}(\xi) = N^K(\xi)\overline{\mathbf{x}}_K \tag{4.54}$$

$$\mathbf{x}(\xi) = N^K(\xi)\mathbf{x}_K \tag{4.55}$$

The summation convention is being used above.

4.5 Transformation due to Boundary Conditions

The transformation required in the beam boundary conditions is a little tricky for uniform splines. This is because of the presence of ghost nodes. In this section a simple method is described in order to apply boundary condition in this kind of problem.

Since the beam is divided into n equally sized elements, there are totally $n+3$ spline parameters to define the displacement functions, including two end spline parameters. That includes $n+1$ usual nodes from $\mathbf{x}_1$ to $\mathbf{x}_{n+1}$ and 2 ghost nodes one at beginning and other at the end. This is because each element is discretized into 4 nodes. Lets say the ghost nodes are denoted by: $\mathbf{x}_0$ and $\mathbf{x}_{n+2}$. In order to apply boundary conditions in a proper way, the end ghost nodal position vectors are needed to be transformed accordingly. For example, the displacement vector in a clamped pinned beam looks is transformed from $\mathbf{x} = [x_0,x_1,x_2....,x_n,x_{n+1},x_{n+2}]$ to $\hat{\mathbf{x}} = [x_0,x_0',x_2....x_n,x_{n+1},x_{n+1}'']$. By taking the boundary conditions into consideration, x_0,x_0', /x_{n+1} and x_{n+1}' can be expressed in terms of correlative spline parameters, $\mathbf{x}_0 = x_0/6+2x_1/3+x_2/6$, $\mathbf{x}_0' = x_0/2+x_2/2$,$\mathbf{x}_{n+1} = x_n/6+2x_{n+1}/3+x_{n+2}/6$ and $\mathbf{x}_{n+1}'' = x_n-2x_{n+1}+x_{n+2}/6$. Therefore the transformation can be achieved by $\hat{\mathbf{x}} = \mathbf{T}\mathbf{x}$, where $\mathbf{T}$ is the transformation matrix. The the transformed stiffness matrix looks like: $\hat{\mathbf{K}} = (\mathbf{T}^T)^{-1}\mathbf{K}\mathbf{T}^{-1}$. For a clamped pinned beam, the

transformation matrix looks like:

$$\mathbf{T} = \begin{bmatrix} 1/6 & 2/3 & 1/6 & & & & \\ -1/2 & 0 & 1/2 & & & & \\ 0 & 0 & 1 & & & & \\ & & & \ddots & & & \\ & & & & 1 & 0 & 0 \\ & & & & 1/6 & 2/3 & 1/6 \\ & & & & 1 & -2 & 1 \end{bmatrix}$$

5

Sensitivity Analysis

In a structural analysis problem, the first step is the discretization of the structural model using finite elements, finite differences etc. The solution is then found out for the algebric equations. In sensitivity analysis, the means of finding the derivatives of these solution are studied which is needed for various optimization algorithms.

Sensitivity analysis is divided broadly into two types: Discrete and Continuum. The difference lies in the step when the differentiation with the design variable is performed. In the discrete approach, first the discretization is done and then differentiation is performed, whereas in the variational approach or continuum approach, governing equations are first differentiated followed by discretization. In addition, under each category there are two general ways of performing sensitivity analysis: the direct method and the adjoint method. The discrete type sensitivity can also be calculated sensitivity using global finite differences. Further direct and adjoint formulations could be subdivided into semi-analytical and analytical methods. Figure 5.1 illustrates all methods of sensitivity analysis briefed above.

5.1 Discrete Sensitivity Analysis by Global Finite Differences

In this method, the derivatives of the response function with respect to the design variables are found with the help of finite difference scheme. This is conceptually very simple, however, could be computationally very expensive when the numbers of design variables are too high. The finite difference scheme using forward difference could be

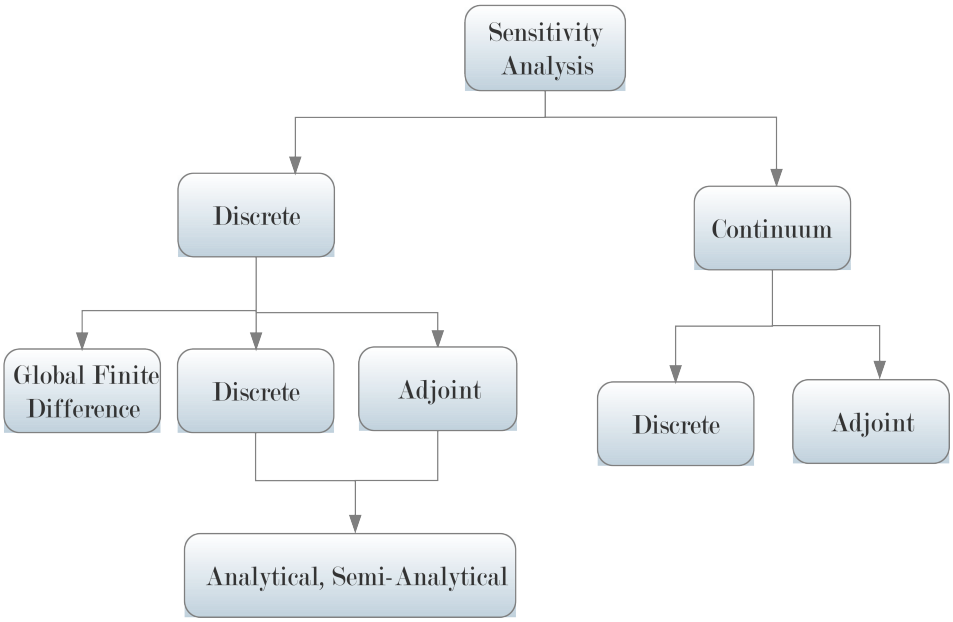

Figure 5.1: Methods for Sensitivity Analysis

shown as the following:

$$\frac{\partial\psi(\mathbf{s})}{\partial\mathbf{s}_i} \approx \frac{\Delta\psi(\mathbf{s}_1,...\mathbf{s}_{ns})}{\Delta\mathbf{s}_i} = \frac{\psi(\mathbf{s}_1,...,\mathbf{s}_i+\Delta\mathbf{s}_i,...\mathbf{s}_{ns}) - \psi(\mathbf{s}_1,...,\mathbf{s}_i,...\mathbf{s}_{ns})}{\Delta\mathbf{s}_i} + O(\Delta\mathbf{s}_i) \quad (5.1)$$

where $O(\Delta\mathbf{s}_i)$ is the truncation error given by:

$$O(\Delta\mathbf{s}_i) = -\frac{\Delta\mathbf{s}_i}{2}\frac{\partial^2\psi}{\partial\mathbf{s}_i^2}\bigg|_{(\mathbf{s}_1,...\mathbf{s}_i+\varepsilon\Delta\mathbf{s}_i,...\mathbf{s}_{ns})} \quad (5.2)$$

with $0 \leq \varepsilon \leq 1$

It can be deduced from (5.1) that it is necessary to evaluate for an additional perturbed design with $\mathbf{s}_i + \Delta\mathbf{s}_i$, in order to compute sensitivity $\partial\psi(\mathbf{s})/\partial\mathbf{s}_i$. The global finite difference method requires *ns* additional analysis of perturbed designs, if sensitivities of ψ are to be computed with respect to *ns* design variables. Thus, this method is quite computationally expensive.

The step size chosen for the design variable affects the accuracy of the results. The smaller the step size better is the approximation, and more accurate the results comes out to be. However, for very small size step, round off errors may creep in. It should be also be noted that for the correct functioning of this method, one should check that there should convergence in the solution after a certain size step.

This method was used widely in the past because of its simple implementation. However, with the development of more accurate and fast techniques, its use has been formidably

reduced. But, it still remains a reference method for validating other implementations. One of the other popular alternatives to global finite difference is Discrete Direct method and Adjoint Method, which is discussed in the following sections.

5.2 Discrete Direct Sensitivity Analysis

In the discrete sensitivity approach, also known as implicit sensitivity approach, the governing equations are first discretized and then differentiated analytically with respect to the design variables. In the discretization process geometry and displacements are approximated by a linear combination of global shape functions.

A general objective function in a sensitivity analysis looks like:

$$\psi = \psi(\mathbf{s},\mathbf{u}) \tag{5.3}$$

where $\mathbf{s} = \mathbf{s}_i, i = 1...ns$ is the vector of design variables and $\mathbf{u}$ is the vector of displacements. The objective ψ may represent stresses, strains, displacements, reaction forces, etc. Therefore, after discretization, i.e. using Equation 5.1, the functional ψ is approximated by :

$$\psi = \psi(\mathbf{s}, \sum_a \mathbf{N}_a \cdot \mathbf{u}_a) \tag{5.4}$$

In sizing and shape optimization problems,the design variables are geometrical quantities. Thus, the global stiffness matrix and the load vector are functions of these design variables, as in equation below. In order to show the concepts of direct and adjoint optimization, the sensitivity analysis is performed for a linear problem : The governing equations of a linear problem are written as:

$$\mathbf{K}(\mathbf{s}) \cdot \mathbf{u}(\mathbf{s}) = \mathbf{F}(\mathbf{s}) \tag{5.5}$$

the vector of displacements obtained as solution to the structural analysis also depends on the design variables,that is $\mathbf{u} = \mathbf{u}(\mathbf{s})$ Considering this, the derivative of the functional ψ as in Equation (5.3) with respect to the vector of design variables $\mathbf{s}$ using chain rule is given by:

$$\frac{\mathrm{d}\psi}{\mathrm{d}\mathbf{s}} = \frac{\partial\psi}{\partial\mathbf{s}} + \frac{\partial\psi}{\partial\mathbf{u}}.\frac{\partial\mathbf{u}}{\partial\mathbf{s}} \tag{5.6}$$

It should be noted that here the shape functions doesn't depend upon the design variables, and its derivative with respective to design variable will be zero. Derivatives $\partial\psi/\partial\mathbf{s}$ and $\partial\psi/\partial\mathbf{u}$ are determined explicitly. The computation of derivatives of the state variables, that is $\partial\mathbf{u}/\partial\mathbf{s}$, is the main task of discrete sensitivity analysis.

Based on the way to organize the operations, it can be distinguished between direct and adjoint sensitivity analysis. In both cases, the computation of the so-called pseudo load vector, which will be introduced next, is required. Depending on the way the pseudo load vector is computed, semi-analytical and analytical sensitivities can be distinguished.

For discrete direct sensitivity analysis, the system equilibrium equation 5.6 must be differentiated with respect to the design variable $\mathbf{s}_i$.

$$\mathbf{K} \cdot \frac{\mathrm{d}\mathbf{u}}{\mathrm{d}\mathbf{s}_i} + \frac{\mathrm{d}\mathbf{K}}{d\mathbf{s}_i} \cdot \mathbf{u} = \frac{\mathrm{d}\mathbf{F}}{\mathrm{d}\mathbf{s}_i} \tag{5.7}$$

We define 'Pseudo force' as:

$$\mathbf{K}\frac{\mathrm{d}\mathbf{u}}{\mathrm{d}\mathbf{s}_i} = \mathbf{F}_i^* \tag{5.8}$$

where:

$$\mathbf{F}_i^* = \frac{\mathrm{d}\mathbf{F}}{\mathrm{d}\mathbf{s}_i} - \frac{\mathrm{d}\mathbf{K} \cdot \mathbf{u}}{\mathrm{d}\mathbf{s}_i} \tag{5.9}$$

5.3 Discrete Adjoint Sensitivity Analysis

The alternative approach of adjoint sensitivity is defined in terms of the adjoint variable $\boldsymbol{\lambda}$. Using Equation 5.8 into Equation 5.6 could be written as:

$$\frac{\mathrm{d}\psi}{\mathrm{d}\mathbf{s}_i} = \frac{\partial\psi}{\partial\mathbf{s}_i} + \frac{\partial\psi}{\partial\mathbf{u}} \cdot \mathbf{K}^{-1}(\mathbf{s}) \cdot \mathbf{F}_i^* \tag{5.10}$$

The vector of adjoint variables is defined as:

$$\boldsymbol{\lambda} = \mathbf{K}^{-1}(\mathbf{s}) \cdot \frac{\partial\psi}{\partial\mathbf{u}} \tag{5.11}$$

$$\mathbf{K}(\mathbf{s}) \cdot \boldsymbol{\lambda} = \frac{\partial\psi}{\partial\mathbf{u}} \tag{5.12}$$

The total derivative of functional ψ is given by:

$$\frac{\mathrm{d}\psi}{\mathrm{d}\mathbf{s}_i} = \frac{\partial\psi}{\partial\mathbf{s}_i} + \boldsymbol{\lambda}\mathbf{F}_i^* \tag{5.13}$$

Therefore, a clear distinction can be drawn between the direct and the adjoint method. The difference lies merely in the order in which matrix multiplications in equation (5.12) are executed. In the direct method, first the product $\mathbf{K}^{-1}(\mathbf{s}) \cdot \mathbf{F}_i^*$ is evaluated, whereas in the adjoint approach the product $\partial\psi/\partial\mathbf{s}_i \cdot \mathbf{K}^{-1}(\mathbf{s})$ is evaluated first. This can have a significant effect on the numerical efficiency, depending on the number of design variables compared to the number of response functions. The adjoint method is more efficient

if there are more design variables than response functions, which is usually the case in shape optimization problems. The above pseudo force vector can be calculated using analytical differentiation or numerically. Both the methods are discussed in the next section.

5.4 Semi-Analytical Sensitivity Analysis

The pseudo force vector described above can be calculated both analytically or through finite difference method. As, calculating analytically is a cumbersome process as it might contain complex derivatives, it might be easier to find the derivatives numerically using finite difference with reasonable accuracy. It can be therefore seen as an intermediate technique between the global finite difference scheme and the analytical approach. Many finite differences schemes have been used for numerical evaluation of the pseudo load vector. In the case of forward finite differences, the pseudo load vector is given by :

$$\begin{aligned} \mathbf{F}_i^* &= \frac{\mathrm{d}\mathbf{F}}{\mathrm{d}\mathbf{s}_i} - \frac{\mathrm{d}\mathbf{K}\cdot\mathbf{u}}{\mathrm{d}\mathbf{s}_i} \\ &\approx \frac{\mathbf{F}(s_1,\ldots,s_i+\Delta s_i,\ldots s_{nd}) - \mathbf{F}(\mathbf{s}) - \left(\mathbf{K}(s_1,\ldots,s_i,\ldots s_{ns}) - \mathbf{K}(\mathbf{s})\right)\cdot\mathbf{u}}{\Delta\mathbf{s}_i} \end{aligned} \tag{5.14}$$

where $\Delta\mathbf{s}_i$ is a small but finite increment in design variable $\mathbf{s}_i$. It should be noted that the global pseudo load vector is computed by assembling the individual contributions of the elemental pseudo load vectors.

The basic advantage of semi-analytical sensitivity analysis is that with small programming effort, much better computational efficiency than global finite difference method can be attained. It is slightly difficult to implement than global finite differences, but definitely much easier than analytical method as the complex derivatives of pseudo force terms are not needed to be calculated. Moreover, the semi-analytical approach does not depend on the finite element formulation used. In this context, this is more advantageous than analytical approach that does depend on the finite element formulation used, and therefore, it has to be implemented for each finite element of the code.

However, as it is known, the drawback of finite difference method are approximation errors and round-off errors. Whenever the perturbation $\mathbf{s}_i$ is too large, the derivative suffers from approximation errors. When the perturbation is very small, round-off errors disturb the result. Usually, the range of suitable perturbations has to be investigated for each application. Olhoff and J. (1991) , naming one out of few, had discussed about the inaccuracies of this method and devised numerical techniques to reduce or eliminate them.

5.5 Analytical Sensitivity Analysis

In this method, the pseudo vector is differentiated analytically. The main advantages of this method are its computational efficiency and reliability, and is the most superior among all the methods discussed. As it was already mentioned, sensitivity parameters are needed for the prediction of the structural response of the modified system design in various optimization algorithms. Therefore, accurate sensitivities are important factor to ensure convergence of optimization algorithm and to improve the convergence rate.

A drawback of this approach is that formulation and implementation are more difficult than for the semi-analytical method, and depend on the particular type of finite element used. The analytical differentiation becomes more complex for more complex finite elements. Moreover, in shape optimization, the domain of integration of the also depends on the design variables which introduces additional difficulties. However, once this differentiation is done and implemented in the code, the efficiency and reliability of the computed analytical sensitivities have clear advantage with respect to those computed by the semi-analytical method or global finite difference method. The sensitivities are more complex and difficult for systems where geomterically nonlinearity is included. For those systems,an addition loop for finding equilibirium point is also needed. In Chapter 6, the analytical design sensitivity for the nonlinear beam derived i n Chapter 4 is presented.

6

Analytical Sensitivity of Geometrically Non-linear Problem

In Chapter 5, a review of the different sensitivity analysis methods was presented. The need for more accurate and reliable sensitivity coefficients legitimates the use of the analytical approach. In the previous chapter, the adjoint coefficient was derived for a linear case. However, if even slight nonlinearity in the structural system is introduced, the linear analytical sensitivity doesn't hold valid. With comprehensive application of nonlinear finite element methods nowadays and with advanced computer capabilities, a formulation of nonlinear shape optimization is definitely desired. In order to develop optimal designs of nonlinear structures, it is necessary to formulate design sensitivities of nonlinear structures. Obviously, this method must be efficient and stable for all applications. In order to do so, an understanding of nonlinear finite element procedure is also needed. In this chapter, the design sensitivities for nonlinear structures are derived analytically. Here, the governing equations of nonlinear finite element are solved iteratively until the internal forces are equal to external forces. Newton Raphson method is used to solve such nonlinear problem. The St. Venant-Kirchhoff constitutive equations are used assuming small strains. In addition, the adjoint sensitivity technique is presented with relevance to nonlinear shape optimization. This approach clearly involves higher mathematical complexity but is more efficient and has lower computational costs. With the development of such formulations, the augmentation with existing commercial nonlinear finite element software is easily possible.

6.1 Algorithm

The gradient based approach is used to calculate minimization of objective function. In this thesis, the interior point alogorithm is used to find the optimal shape. 'Interior-point' also referred as barrier method, can be used to solve both linear as well as non-linear constrained optimization problems. Interior point methods are usually solved by applying Newton's method into a sequence of equations containing KKT conditions.

The algorithm satisfies bounds at all iterations, and can recover from Infinite results. The algorithm can use special techniques for large-scale problems. As described in Weisstein "Current efficient implementations are mostly based on a predictor-corrector technique by Mehrotra (1992), where the Cholesky decomposition of the normal equation or LDL^T factorization of the symmetric indefinite system augmented system is used to perform Newton's method (together with some heuristics to estimate the penalty parameter). All current interior point methods implementations rely heavily on very efficient code for factoring sparse symmetric matrices".

The implementation of interior point is not done explicitly, rather, the predefined function in MATLAB called *fmincon* is used in order to calculate the optimal solution. The mathematical details therefore are not discussed this thesis report. The sensitivity information along with the value of objective function is feeded as input variables in the predefined optimization function.

6.2 Analytical Sensitivities

In Chapter 4, the beam element similar to thin shell formulation was studied in detail. In order to use this element for shape optimization, its analytical sensitivities are needed to be computed. Here, the analytical procedure to obtain derivatives are explained. Throughout the section, a continuous reference to matrices and vectors involved in the computation of the element stiffness matrix is made. The objective function is taken as the Strain Energy with the goal of minimizing it. The design variables are the control points of the B-Spline curve.

$$\psi(\mathbf{s},\mathbf{u}) \;=\; \frac{1}{2}\int_{\bar{B}} (\mathbf{S} : \mathbf{E})\, \mathrm{d}\, V \tag{6.1}$$

where the strain energy can be written as:

$$\psi = \frac{1}{2}\int_{\bar{B}} (\mathbf{S} : \mathbf{E})\, \mathrm{d}\, V = \frac{1}{2}\int_{\bar{\Omega}}\int_{h}\int_{b} E_{11}\, C^{1111} E_{11} \mu d\theta^3 d\theta^2 \mathrm{d}\bar{\Omega} \tag{6.2}$$

$$= \frac{1}{2}\int_{\bar{\Omega}}\int_{h}\int_{b} (\alpha + \theta^2\beta)\, C (\alpha + \theta^2\beta) \mu d\theta^3 d\theta^2 \mathrm{d}\bar{\Omega} \tag{6.3}$$

$$= \frac{1}{2}\int_{\bar{\Omega}}\int_{h}\int_{b} (\alpha^2) C + \theta^2 (2.C\alpha\beta) + (\theta^2)^2 (C\beta^2) \mu \mathrm{d}\theta^3 \mathrm{d}\theta^2 \mathrm{d}\bar{\Omega} \tag{6.4}$$

$$= \frac{1}{2}\int_{\bar{\Omega}} (CA\alpha^2 + CI\beta^2) \mathrm{d}\bar{\Omega} \tag{6.5}$$

The equilibrium equations in a nonlinear setting can be written as:

$$\mathbf{f}_{int}(\mathbf{s},\mathbf{u}) - \mathbf{f}_{ext}(\mathbf{s},\mathbf{u}) = 0 \tag{6.6}$$

Using the KKT conditions discussed in Chapter 2, the objective function $\psi(\mathbf{s},\mathbf{u})$ is therefore written as:

$$\psi(\mathbf{s},\mathbf{u}) = \psi + \boldsymbol{\lambda}(\mathbf{f}_{int} - \mathbf{f}_{ext}) \tag{6.7}$$

$$\frac{\mathrm{d}\psi(\mathbf{s},\mathbf{u})}{\mathrm{d}\mathbf{s}_i} = \frac{\partial\psi}{\partial\mathbf{s}_i} + \frac{\partial\psi}{\partial\mathbf{x}_k}\frac{\partial\mathbf{x}_k}{\partial\mathbf{s}_i} + \lambda\left(\frac{\partial\mathbf{f}^{int}}{\partial\mathbf{s}_i} + \frac{\partial\mathbf{f}^{int}}{\partial\mathbf{x}_k}\frac{\partial\mathbf{x}_k}{\partial\mathbf{s}_i} - \frac{\partial\mathbf{f}^{ext}}{\partial\mathbf{s}_i}\right) \tag{6.8}$$

We choose $\boldsymbol{\lambda}$ such that $\partial\mathbf{x}_k/\partial\mathbf{s}_i$ is eliminated. Collecting terms with $\partial\mathbf{x}_k/\partial\mathbf{s}_i$ coefficient

$$\frac{\mathrm{d}\psi(\mathbf{s},\mathbf{u})}{\mathrm{d}\mathbf{s}_i} = \frac{\partial\psi}{\partial\mathbf{s}_i} + \boldsymbol{\lambda}\frac{\partial\mathbf{f}^{int}}{\partial\mathbf{s}_i} - \boldsymbol{\lambda}\frac{\partial\mathbf{f}^{ext}}{\partial\mathbf{s}_i} + \frac{\partial\mathbf{x}_k}{\partial\mathbf{s}_i}\left(\frac{\partial\psi}{\partial\mathbf{x}_k} + \boldsymbol{\lambda}\frac{\partial\mathbf{f}^{int}}{\partial\mathbf{x}_k}\right) \tag{6.9}$$

$$\frac{\partial\psi}{\partial\mathbf{x}_k} + \boldsymbol{\lambda}\frac{\partial\mathbf{f}^{int}}{\partial\mathbf{x}_k} = 0 \tag{6.10}$$

$$\frac{\partial\psi}{\partial\mathbf{x}_k} + \boldsymbol{\lambda}K_t = 0 \tag{6.11}$$

$$\boldsymbol{\lambda} = -\mathbf{K}_T^{-1}\frac{\partial\psi}{\partial\mathbf{x}_k} \tag{6.12}$$

In direct method we first multiply $\mathbf{K}_T^{-1}\left(\partial\mathbf{f}^{int}/\partial\mathbf{s}_i - \partial\mathbf{f}^{ext}/\partial\mathbf{s}_i\right)$ and for adjoint method we first compute $-\mathbf{K}_T^{-1}\partial\psi/\partial\mathbf{x}_k$. However, in this case, as the number of design variables are much larger than the constraints,therefore adjoint method must be used.
If the objective is taken as Strain Energy as described in equation 6.1, the $\boldsymbol{\lambda}$ turns out to be:

$$\boldsymbol{\lambda} = -\mathbf{K}_T^{-1}\mathbf{f}^{int} \tag{6.13}$$

Substituting $\boldsymbol{\lambda}$ into 6.8, we get:

$$\frac{\mathrm{d}\psi(\mathbf{s},\mathbf{u})}{d\mathbf{s}_i} = \frac{\partial\psi}{\partial\mathbf{s}_i} - \mathbf{K}_T^{-1}\mathbf{f}^{int}\left(\frac{\partial\mathbf{f}^{int}}{\partial\mathbf{s}_i} - \frac{\partial\mathbf{f}^{ext}}{\partial\mathbf{s}_i}\right) \tag{6.14}$$

Therefore, in order to computer the sensitivity of Strain Energy, $\frac{\partial\psi}{\partial\mathbf{s}_i}$,$\frac{\partial\mathbf{f}^{int}}{\partial\mathbf{s}_i}$ and $\frac{\partial\mathbf{f}^{ext}}{\partial\mathbf{s}_i}$ needs to be computed.

Calculation of $\partial\psi/\partial\mathbf{s}_i$:

$$\begin{aligned}\psi = \frac{1}{2}\int_{\bar{B}}(\mathbf{S}:\mathbf{E})\,dV &= \frac{1}{2}\int_{\bar{\Omega}}\int_h\int_b E_{11}C^{1111}E_{11}\mu\mathrm{d}\theta^3\mathrm{d}\theta^2\mathrm{d}\bar{\Omega} \\ &= \frac{1}{2}\int_{\bar{\Omega}}\int_h\int_b E_{11}C^{1111}E_{11}\mu\mathrm{d}\theta^3\mathrm{d}\theta^2|\mathbf{a}_1|\mathrm{d}\theta^1\end{aligned} \tag{6.15}$$

$$\begin{aligned}\frac{\partial\psi}{\partial\mathbf{s}_i} =& \frac{1}{2}\int_{\bar{\Omega}}\int_h\int_b \frac{\partial E_{11}}{\partial s_i}C^{1111}E_{11}\mu|\mathbf{a}_1|\mathrm{d}\theta^3\mathrm{d}\theta^2\mathrm{d}\theta^1 + \\ & \frac{1}{2}\int_{\bar{\Omega}}\int_h\int_b E_{11}\frac{\partial C^{1111}}{\partial s_i}E_{11}\mu|\mathbf{a}_1|\mathrm{d}\theta^3\mathrm{d}\theta^2\mathrm{d}\theta^1 + \\ & \frac{1}{2}\int_{\bar{\Omega}}\int_h\int_b E_{11}C^{1111}\frac{\partial E_{11}}{\partial\mathbf{s}_i}\mu|\mathbf{a}_1|\mathrm{d}\theta^3\mathrm{d}\theta^2\mathrm{d}\theta^1 + \\ & \frac{1}{2}\int_{\bar{\Omega}}\int_h\int_b E_{11}C^{1111}E_{11}\frac{\partial\mu}{\partial s_i}|\mathbf{a}_1|\mathrm{d}\theta^3\mathrm{d}\theta^2\mathrm{d}\theta^1 + \\ & \frac{1}{2}\int_{\bar{\Omega}}\int_h\int_b E_{11}C^{1111}E_{11}\mu\frac{\partial|\mathbf{a}_1|}{\partial\mathbf{s}_i}\mathrm{d}\theta^3\mathrm{d}\theta^2\mathrm{d}\theta^1\end{aligned} \tag{6.16}$$

As mentioned in Chapter 4 (Equation 4.20), μ is taken as 1 and therefore $\partial\mu/\partial\mathbf{s}_i$ is taken as zero. Therefore the above equation simplifies to:

$$\begin{aligned}\frac{\partial\psi}{\partial\mathbf{s}_i} =& \int_{\bar{\Omega}}\int_h\int_b \frac{\partial E_{11}}{\partial\mathbf{s}_i}C^{1111}E_{11}\mu|\mathbf{a}_1|\mathrm{d}\theta^3\mathrm{d}\theta^2\mathrm{d}\theta^1 + \\ & \frac{1}{2}\int_{\bar{\Omega}}\int_h\int_b E_{11}\frac{\partial C^{1111}}{\partial\mathbf{s}_i}E_{11}\mu|\mathbf{a}_1|\mathrm{d}\theta^3\mathrm{d}\theta^2\mathrm{d}\theta^1 + \\ & \frac{1}{2}\int_{\bar{\Omega}}\int_h\int_b E_{11}C^{1111}E_{11}\mu\frac{\partial|\mathbf{a}_1|}{\partial\mathbf{s}_i}\mathrm{d}\theta^3\mathrm{d}\theta^2\mathrm{d}\theta^1\end{aligned} \tag{6.17}$$

where

$$\int_{\bar{\Omega}}\int_{h}\int_{b}\frac{\partial E_{11}}{\partial \mathbf{s}_i}C^{1111}E_{11}\mu|\mathbf{a}_1|\mathrm{d}\theta^3\mathrm{d}\theta^2\mathrm{d}\theta^1 = \int_{\overline{\Omega}}\int_{h}\int_{b}(\alpha+\theta^2\beta)C(\frac{\partial\alpha}{\partial\mathbf{s}_i}+\theta^2\frac{\partial\beta}{\partial\mathbf{s}_i})\overline{\mu}|\mathbf{a}_1|\mathrm{d}\theta^3\mathrm{d}\theta^2\mathrm{d}\theta^1$$
$$=\int_{\overline{\Omega}}\int_{h}\int_{b}\left(\alpha C\frac{\partial\alpha}{\partial\mathbf{s}_i}+\theta^2(\beta C\frac{\partial\alpha}{\partial\mathbf{s}_i}+\alpha C\frac{\partial\beta}{\partial\mathbf{s}_i})+(\theta^2)^2\beta C\frac{\partial\beta}{\partial\mathbf{s}_i}\right)\overline{\mu}|\mathbf{a}_1|\mathrm{d}\theta^3\mathrm{d}\theta^2\mathrm{d}\theta^1 \tag{6.18}$$

Note that the above functon integrals over the cross section can be evaluated analytically, which leads to

$$= \int_{\omega}\left(CA\alpha\frac{\partial\alpha}{\partial\mathbf{s}_i}+CI\beta\frac{\partial\beta}{\partial\mathbf{s}_i}\right)|\mathbf{a}_1|\mathrm{d}\theta^1+\int_{\omega}\left(CI\beta\frac{\partial\alpha}{\partial\mathbf{s}_i}+CI\alpha\frac{\partial\beta}{\partial\mathbf{s}_i}\right)\overline{\mu}|\mathbf{a}_1|\mathrm{d}\theta^1 \tag{6.19}$$

Similarly the second term of eq 6.17 can be simplified as follows:

$$\frac{1}{2}\int_{\bar{\Omega}}\int_{h}\int_{b}E_{11}\frac{\partial C^{1111}}{\partial\mathbf{s}_i}E_{11}\mu|\mathbf{a}_1|\mathrm{d}\theta^3\mathrm{d}\theta^2\mathrm{d}\theta^1=\frac{1}{2}\int_{\bar{\Omega}}\int_{h}\int_{b}E_{11}\frac{\partial}{\partial\mathbf{s}_i}\left(\frac{\mathbb{E}}{\overline{g}_{11}\overline{g}_{11}}\right)E_{11}\mu|\mathbf{a}_1|\mathrm{d}\theta^3\mathrm{d}\theta^2\mathrm{d}\theta^1 \tag{6.20}$$

where $\mathbb{E}$ is Young's modulus and $\overline{g}^{11}$ is the 11-entry of the contra-variant metric coefficients. Note, $\overline{g}^{11}$ depends in general on θ^1 and θ^2. As, derived in Section 4.2 (Equation 4.19), $\overline{g}^{11}$ can be written as:

$$\overline{g}_{11}=|\overline{\mathbf{a}}_1|^2+2\theta^2\overline{\mathbf{a}}_1\cdot\overline{\mathbf{a}}_2'+(\theta^2)^2\left(\frac{\overline{\mathbf{a}}_2'\cdot\overline{\mathbf{a}}_2'}{|\overline{\mathbf{a}}_1|}\right)^2 \tag{6.21}$$

Neglecting the quadratic term, we find the derivative of the term $\mathbb{E}/\overline{g}_{11}\overline{g}_{11}$ with respect to design variable:

$$\frac{\partial}{\partial\mathbf{s}_i}\left(\frac{\mathbb{E}}{\overline{g}_{11}\overline{g}_{11}}\right)=\frac{-2\mathbb{E}}{{\overline{g}_{11}}^3}\left(2|\overline{\mathbf{a}}_1|\frac{\partial|\overline{\mathbf{a}}_1|}{\partial\mathbf{s}_i}+2\theta^2\big(\overline{\mathbf{a}}_1\cdot\frac{\partial\overline{\mathbf{a}}_2'}{\partial\mathbf{s}_i}+\overline{\mathbf{a}}_2'\cdot\frac{\partial\overline{\mathbf{a}}_1}{\partial\mathbf{s}_i}\big)\right) \tag{6.22}$$

The above equation can be written in a simplified form say:

$$\begin{aligned}\frac{\partial}{\partial\mathbf{s}_i}\left(\frac{\mathbb{E}}{\overline{g}_{11}\overline{g}_{11}}\right) &= X+\theta^2\,Y\\ X &= \frac{-4\mathbb{E}}{{\overline{g}_{11}}^3}\left(|\overline{\mathbf{a}}_1|\frac{\partial|\overline{\mathbf{a}}_1|}{\partial s_i}\right)\\ Y &= \frac{-4\mathbb{E}}{{\overline{g}_{11}}^3}\left(\overline{\mathbf{a}}_1\cdot\frac{\partial\overline{\mathbf{a}}_2'}{\partial\mathbf{s}_i}+\overline{\mathbf{a}}_2'\cdot\frac{\partial\overline{\mathbf{a}}_1}{\partial\mathbf{s}_i}\right)\end{aligned} \tag{6.23}$$

On substituting the Equation 4.14 containing the components of Green Lagrange strain and using 6.23, Equation 6.20 can be written as:

$$\frac{1}{2}\int_{\bar{\Omega}}\int_{h}\int_{b} E_{11}\frac{\partial C^{1111}}{\partial \mathbf{s}_i}E_{11}\mu|\mathbf{a}_1|\mathrm{d}\theta^3\mathrm{d}\theta^2\mathrm{d}\theta^1 = \frac{1}{2}\int_{\omega}\int_{h}\int_{b}(\alpha+\theta^2\beta)(X+\theta^2 Y)(\alpha+\theta^2\beta)\mu|\mathbf{a}_1|\mathrm{d}\theta^3\mathrm{d}\theta^2\mathrm{d}\theta^1 \tag{6.24}$$

This could be further expanded as:

$$\begin{aligned} &= \frac{1}{2}\int_{\omega}\int_{h}\int_{b}\Big((\alpha^2 X+(\theta^2)^2(\beta^2 X+2\alpha\beta Y))+(\theta^2)(2\alpha\beta X+\alpha^2 Y)+ \\ &\qquad (\theta^2)^3(\beta^2 Y)\Big)\mu|\mathbf{a}_1|\mathrm{d}\theta^3\mathrm{d}\theta^2\mathrm{d}\theta^1 \\ &= \frac{1}{2}\int_{\omega}\Big(AX\alpha^2+I(X\beta^2+2Y\alpha\beta)\Big)|\mathbf{a}_1|\mathrm{d}\theta^3\mathrm{d}\theta^2\mathrm{d}\theta^1+ \\ &\qquad \frac{1}{2}\int_{\omega}\Big(I(2\alpha\beta X+\alpha^2 Y)\Big)\eta|\mathbf{a}_1|\mathrm{d}\theta^3\mathrm{d}\theta^2\mathrm{d}\theta^1 \end{aligned} \tag{6.25}$$

where $A = bh$ is the area of the cross section and $I = bh^3/12$ is the moment of inertia of the cross section. The second integral is neglected, it is only present in initially curved beams. Further, the membrane force is defined as $n = CA\alpha$ and the couple force as $m = CA\beta$. The odd powers of θ^2 cancels out as the result in zero on integration. Therefore, the second term of Equation 6.17 can be finally written as:

$$\frac{1}{2}\int_{\bar{\Omega}}\int_{h}\int_{b} E_{11}\frac{\partial C^{1111}}{\partial \mathbf{s}_i}E_{11}\mu|\mathbf{a}_1|\mathrm{d}\theta^3\mathrm{d}\theta^2\mathrm{d}\theta^1 = \frac{1}{2}\int_{\omega}\Big(AX\alpha^2+I(X\beta^2+2Y\alpha\beta)\Big)|\mathbf{a}_1|\mathrm{d}\theta^3\mathrm{d}\theta^2\mathrm{d}\theta^1 \tag{6.26}$$

where X and Y are defined in Equation 6.23. For the calculation of X and Y, the sensitivities of $|\mathbf{a}_1|$,$\mathbf{a}_1$ and **a2** needs to be calculated. For this the Appendix as well as section 6.3.1 must be referred.
Next, the third term in Equation 6.17 is needes to be computer. This is quite simple as only $\partial|\mathbf{a}_1|/\partial\mathbf{s}_i$ needs to be computed, which is shown in Appendix A and rest of the terms are already known.

Calculation of $\partial \mathbf{f}^{int}/\partial \mathbf{s}_i$: Using Equation 4.20 in 4.34 and then taking the derivative of Equation 4.34 with the design variable, the obtained equation takes the form:

$$\begin{aligned}\frac{\partial \mathbf{f}^{int}}{\partial s_i} &= \frac{\partial}{\partial \mathbf{s}_i}\int_{\omega}\int_{h}\int_{b} E^{11}\, C \frac{\partial E^{11}}{\partial \mathbf{x}_K}\mu|\mathbf{a}_1|\mathrm{d}\theta^3\mathrm{d}\theta^2\mathrm{d}\theta^1 \\ &= \frac{\partial}{\partial \mathbf{s}_i}\int_{\omega}\int_{h}\int_{b}(\alpha+\theta^2\beta)\, C(\frac{\partial \alpha}{\partial \mathbf{x}_K}+\theta^2\frac{\partial \beta}{\partial \mathbf{x}_K})\mu|\mathbf{a}_1|\mathrm{d}\theta^3\mathrm{d}\theta^2\mathrm{d}\theta^1\end{aligned} \tag{6.27}$$

Differentiating all the terms,

$$\begin{aligned}\frac{\partial \mathbf{f}^{int}}{\partial \mathbf{s}_i} &= \int_{\omega}\int_{h}\int_{b}(\frac{\partial \alpha}{\partial \mathbf{s}_i}+\theta^2\frac{\partial \beta}{\partial \mathbf{s}_i})\, C(\frac{\partial \alpha}{\partial \mathbf{x}_K}+\theta^2\frac{\partial \beta}{\partial \mathbf{x}_K})\mu|\mathbf{a}_1|\mathrm{d}\theta^3\mathrm{d}\theta^2\mathrm{d}\theta^1 \\ &+ \int_{\omega}\int_{h}\int_{b}(\alpha+\theta^2\beta)\frac{\partial C}{\partial \mathbf{s}_i}(\frac{\partial \alpha}{\partial \mathbf{x}_K}+\theta^2\frac{\partial \beta}{\partial \mathbf{x}_K})\mu|\mathbf{a}_1|\mathrm{d}\theta^3\mathrm{d}\theta^2\mathrm{d}\theta^1 \\ &+ \int_{\omega}\int_{h}\int_{b}(\alpha+\theta^2\beta)\, C\left(\frac{\partial}{\partial s_i}(\frac{\partial \alpha}{\partial \mathbf{x}_K}+\theta^2\frac{\partial \beta}{\partial \mathbf{x}_K})\right)\mu|\mathbf{a}_1|\mathrm{d}\theta^3\mathrm{d}\theta^2\mathrm{d}\theta^1 \\ &+ \int_{\omega}\int_{h}\int_{b}(\alpha+\theta^2\beta)\, C(\frac{\partial \alpha}{\partial \mathbf{x}_K}+\theta^2\frac{\partial \beta}{\partial \mathbf{x}_K})\mu\frac{\partial|\mathbf{a}_1|}{\partial s_i}\mathrm{d}\theta^3\mathrm{d}\theta^2\mathrm{d}\theta^1\end{aligned} \tag{6.28}$$

As the design parameters are taken as initial nodal coordinates, the term $\partial/\partial \mathbf{s}_i\Big(\partial\alpha/\partial \mathbf{x}_K + \theta^2\partial\beta/\partial \mathbf{x}_K\Big)$ is zero
The first term of Equation 6.29 can be simplified as:

$$\begin{aligned}&\int_{\omega}\int_{h}\int_{b}(\frac{\partial \alpha}{\partial \mathbf{s}_i}+\theta^2\frac{\partial \beta}{\partial \mathbf{s}_i})\, C(\frac{\partial \alpha}{\partial \mathbf{x}_K}+\theta^2\frac{\partial \beta}{\partial \mathbf{x}_K})\mu|\mathbf{a}_1|\mathrm{d}\theta^3\mathrm{d}\theta^2\mathrm{d}\theta^1 \\ &= \int_{\omega}\int_{h}\int_{b}\left(\frac{\partial \alpha}{\partial \mathbf{s}_i}C\frac{\partial \alpha}{\partial \mathbf{x}_K}+(\theta^2)^2\frac{\partial \beta}{\partial \mathbf{s}_i}C\frac{\partial \beta}{\partial \mathbf{x}_K}+\theta^2 C(\frac{\partial \alpha}{\partial \mathbf{s}_i}\frac{\partial \beta}{\partial \mathbf{x}_K}+\frac{\partial \beta}{\partial \mathbf{s}_i}\frac{\partial \alpha}{\partial \mathbf{x}_K})\right)\mu|\mathbf{a}_1|\mathrm{d}\theta^3\mathrm{d}\theta^2\mathrm{d}\theta^1 \\ &= \int_{\omega}\left(CA\frac{\partial \alpha}{\partial \mathbf{s}_i}\frac{\partial \alpha}{\partial \mathbf{x}_K}+CI\frac{\partial \beta}{\partial \mathbf{s}_i}\frac{\partial \beta}{\partial \mathbf{x}_K}\right)|\mathbf{a}_1|\mathrm{d}\theta^1+\int_{\omega}\left(CI(\frac{\partial \alpha}{\partial \mathbf{s}_i}\frac{\partial \beta}{\partial \mathbf{x}_K}+\frac{\partial \beta}{\partial s_i}\frac{\partial \alpha}{\partial \mathbf{x}_K})\right)\overline{\eta}|\mathbf{a}_1|\mathrm{d}\theta^1\end{aligned} \tag{6.29}$$

The second term comes to be zero as et is zero for straight beams. Now, the second term of Equation 6.29 can be written as:

$$\begin{aligned}
&\int_{\omega}\int_{h}\int_{b}(\alpha+\theta^2\beta)\frac{\partial C}{\partial \mathbf{s}_i}(\frac{\partial \alpha}{\partial \mathbf{x}_K}+\theta^2\frac{\partial \beta}{\partial \mathbf{x}_K})\mu|\mathbf{a}_1|\mathrm{d}\theta^3\mathrm{d}\theta^2\mathrm{d}\theta^1 \\
&=\int_{\omega}\int_{h}\int_{b}(\alpha+\theta^2\beta)(X+\theta^2 Y)(\frac{\partial \alpha}{\partial \mathbf{x}_K}+\theta^2\frac{\partial \beta}{\partial \mathbf{x}_K})\mu|\mathbf{a}_1|\mathrm{d}\theta^3\mathrm{d}\theta^2\mathrm{d}\theta^1 \\
&=\frac{1}{2}\int_{\omega}\int_{h}\int_{b}\Bigg((\alpha X\frac{\partial \alpha}{\partial \mathbf{x}_K}+(\theta^2)^2(\beta Y\frac{\partial \alpha}{\partial \mathbf{x}_K})+(\theta^2)^2(\alpha Y+\beta X)\frac{\partial \beta}{\partial \mathbf{x}_K}+ \\
&\cancel{(\theta^2)(\alpha Y+\beta X)\frac{\partial \alpha}{\partial \mathbf{x}_K}}+\cancel{(\theta^2)\alpha X\frac{\partial \beta}{\partial \mathbf{x}_K}}+\cancel{(\theta^2)^3(\beta^2 Y)}\Bigg)\mu|\mathbf{a}_1|\mathrm{d}\theta^3\mathrm{d}\theta^2\mathrm{d}\theta^1 \\
&=\frac{1}{2}\int_{\omega}\left(A\alpha X\frac{\partial \alpha}{\partial \mathbf{x}_K}+I(\beta Y\frac{\partial \alpha}{\partial \mathbf{x}_K})+I(\alpha Y+\beta X)\frac{\partial \beta}{\partial \mathbf{x}_K}\right)|\mathbf{a}_1|\mathrm{d}\theta^1
\end{aligned} \tag{6.30}$$

Here calculation of $\partial|\overline{\mathbf{a}}_1|/\partial \mathbf{s}_i$ can be found in Appendix.

6.2.1 Sensitivity of Strain Components

Differentiation of different strain component with design variable is found out to be:

$$\begin{aligned}
\frac{\partial \alpha}{\partial \mathbf{s}_i}&=-\overline{\mathbf{a}}_1\cdot\frac{\partial \overline{\mathbf{a}}_1}{\partial \mathbf{s}_i} \\
\frac{\partial \beta}{\partial \mathbf{s}_i}&=\overline{\mathbf{a}}_2\cdot\frac{\partial \overline{\mathbf{a}}_1'}{\partial \mathbf{s}_i}+\overline{\mathbf{a}}_1'\cdot\frac{\partial \overline{\mathbf{a}}_2}{\partial \mathbf{s}_i}
\end{aligned} \tag{6.31}$$

The sensitivity of the tangent vector yields to:

$$\frac{\partial \overline{\mathbf{a}}_1}{\partial \mathbf{s}_i}=N'^J\mathbf{I} \tag{6.32}$$

and the normal vector result in

$$\frac{\partial \overline{\mathbf{a}}_2}{\partial \mathbf{x}_K}=\frac{1}{|\overline{\mathbf{a}}_1|}\overline{\mathbf{a}}_3\times\frac{\partial \overline{\mathbf{a}}_1}{\partial \mathbf{s}_i}-\overline{\mathbf{a}}_2\left(\frac{\overline{\mathbf{a}}_1}{|\overline{\mathbf{a}}_1|^2}\cdot\frac{\partial \overline{\mathbf{a}}_1}{\partial \mathbf{s}_i}\right) \tag{6.33}$$

The sensitivity of the derived tangent vector is straight forward

$$\frac{\partial \mathbf{a}_1'}{\partial \mathbf{s}_i}=N''^J\mathbf{I} \tag{6.34}$$

With this, all the terms in Equation 6.14 can be computed and thus the sensitivity of the objective function can be calculated. In order to correctly find the derivatives, each terms were checked with finite differences.

7

Results

In this Chapter, numerical examples are presented on isogeometric analysis using uniform B-Splines and on nonlinear shape optimization of beams for large deformations. This Chapter is divided broadly into three parts: Linear Analysis, Nonlinear Analysis and Optimization. The code is first validated by taking some examples of linear and geomterically nonlinear beam problems. Then, in the final section, some beam problems are taken where the optimized shapes are found for some general load cases. A validation of the formulation is performed by camparing the shape with the inverted catenary curve. The effect of optimized shape is also studied on changing different parameters like number of elements, thickness to length ratio and on increasing load. To study the shape of a beam in the geometrical nonlinear regime, a problem of beam buckling on a point load is taken.

7.1 Linear problem

In this section, some simple analysis problems were solved using the beam equations formulated with uniform B-Splines in Chapter 4. This was done in order to check the proper functionality of the code for linear cases. The beam was discretized with 4 and 16 elements, and for various support cases, as shown in Fig 7.1. The finite element solution was then compared with the analytical solution.

The mesh in both the cases: 4 and 16 elements is depicted in Figute 7.2. As for B-Splines, additional ghost nodes one at the beginning and other at the end, are needed for the interpolation. This is because a single element is described by four points. So, for the first and last element, extra nodes are required. The geometric properties are:

E = 1000, A = 0.02, I = 1.333×10^5, $\hat{p} = 0.0002$, L = 4.

Table 7.1 shows the comparision of displacement at $x = L/2$ using finite element result with 4 and 16 elements and with the analytical solution. Figure 7.1. In Fig 7.3 to Fig 7.5, the support conditions are as follows:

$$clamped - free \qquad u_0 = u_0' = 0.0 \qquad u_L'' = u_L''' = 0.0 \tag{7.1}$$

$$clamped - clamped \qquad u_0 = u_0' = 0.0 \qquad u_L = u_L' = 0.0 \tag{7.2}$$

$$clamped - pinned \qquad u_0 = u_0' = 0.0 \qquad u_L = u_L' = 0.0 \tag{7.3}$$

The analytical equation for the deflection at any length x from the beginning of the beam for clamped at one end and free in another is given by:

$$u(x) = \frac{p}{24EI}(x^4 - 4Lx^3 + 6L^2x^2) \tag{7.4}$$

Similary to clamped-clamped boundary condition, the analytical solution for the deflection is as follows:

$$u(x) = \frac{p}{24EI}(x^4 - 2Lx^3 + L^2x^2) \tag{7.5}$$

and for clamped pinned, the analytical solution is given as:

$$u(x) = \frac{p}{48EI}(2x^4 - 5Lx^3 + 3L^2x^2) \tag{7.6}$$

The solution from the isogeometric solution was then compared with these analytical solution for these particular cases. Its is quite clear from the comparision that, even for just 4 elements, the B-Spline discretization gives quite accurate results. This validates the code of isogeometric analysis using uniform B-Splines in a linear static case.

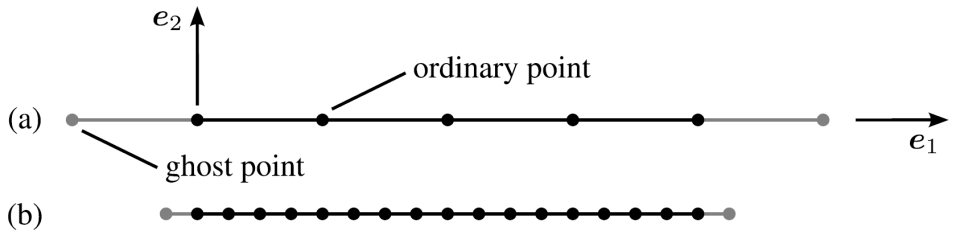

Figure 7.1: Single-span meshes: (a) mesh with 4 and (b) with 16 uniform elements

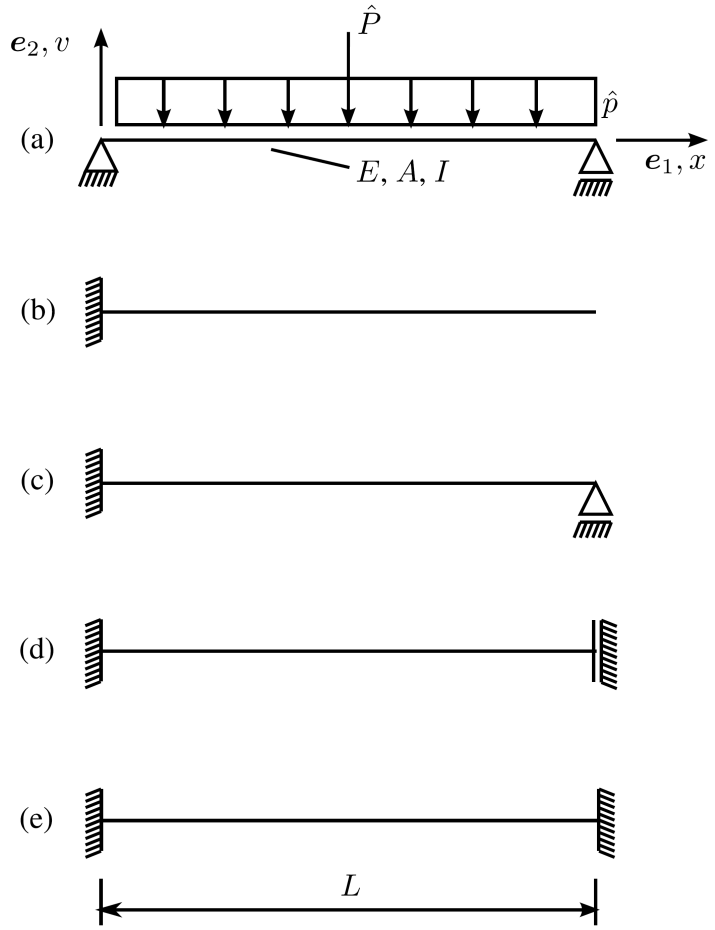

Figure 7.2: Problem definition for Linear single span systems

System	Analytical Value	Figure 7.1(a)	Figure 7.1(b)
Figure 7.1(a)	-0.05	-0.05	-0.05
Figure 7.1(b)	-0.17	-0.17	-0.17
Figure 7.1(c)	-0.02	-0.02	-0.02
Figure 7.1(d)	-0.09	-0.09	-0.09
Figure 7.1(e)	-0.01	-0.01	-0.01

Table 7.1: Results for E = 1000, A = 0.02, I = $1.333.10^5$, $\hat{p} = 0.0002$, L = 4 at x = L/2

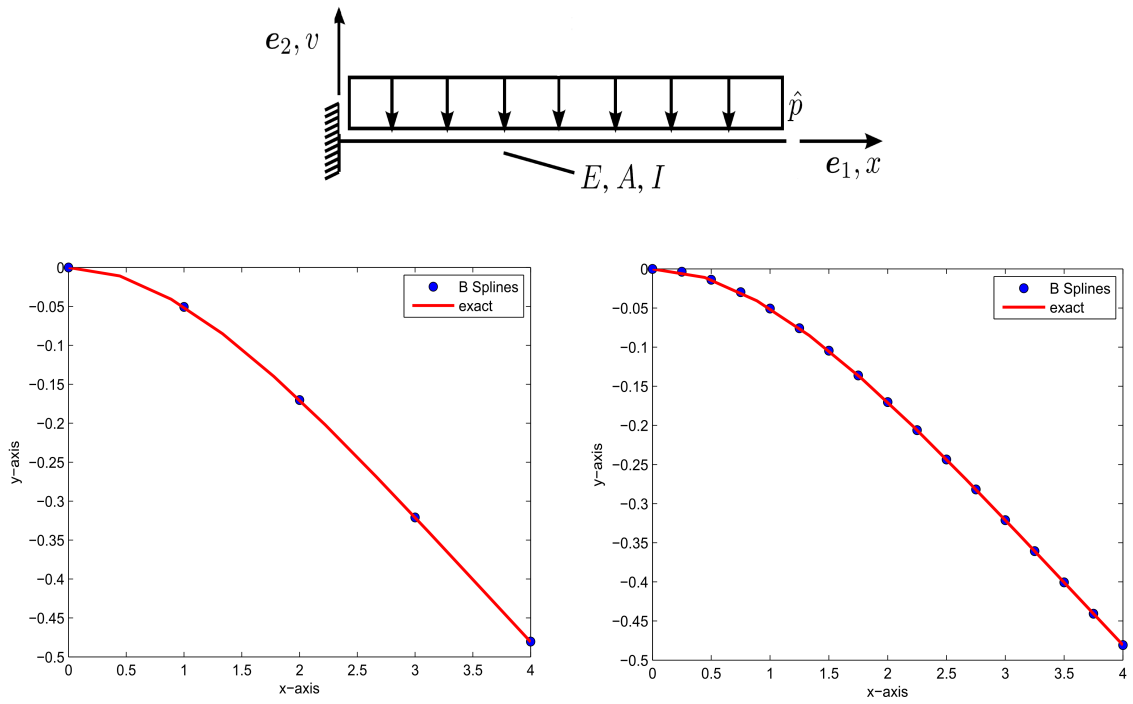

Figure 7.3: Clamped-Free: (a) mesh with 4 and (b) with 16 uniform elements

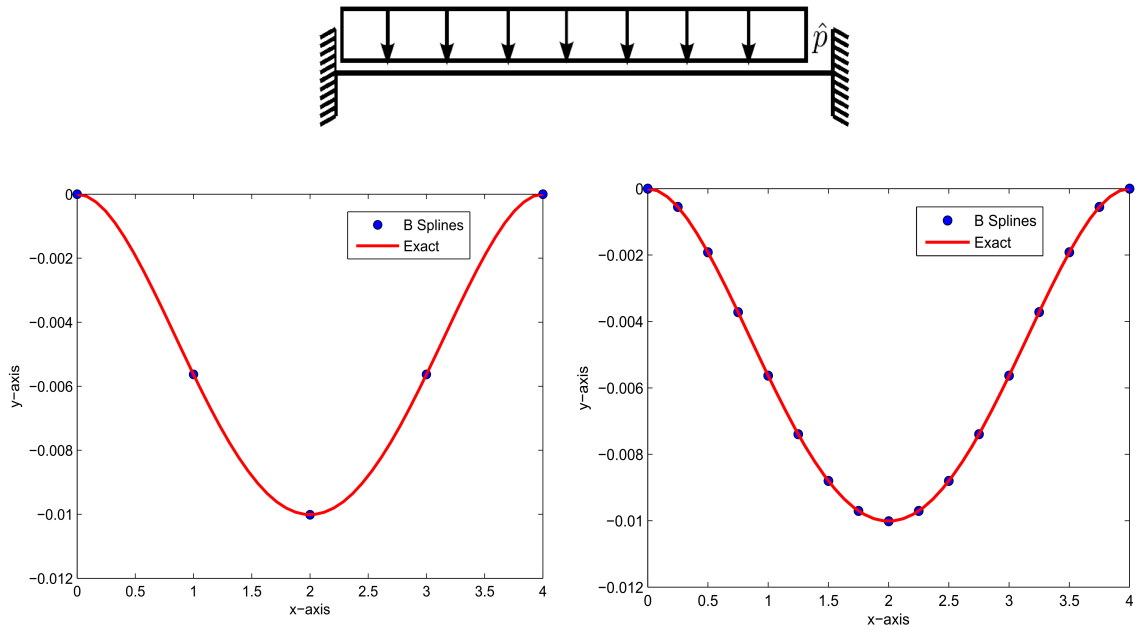

Figure 7.4: Clamped-Clamped: (a) mesh with 4 and (b) with 16 uniform elements

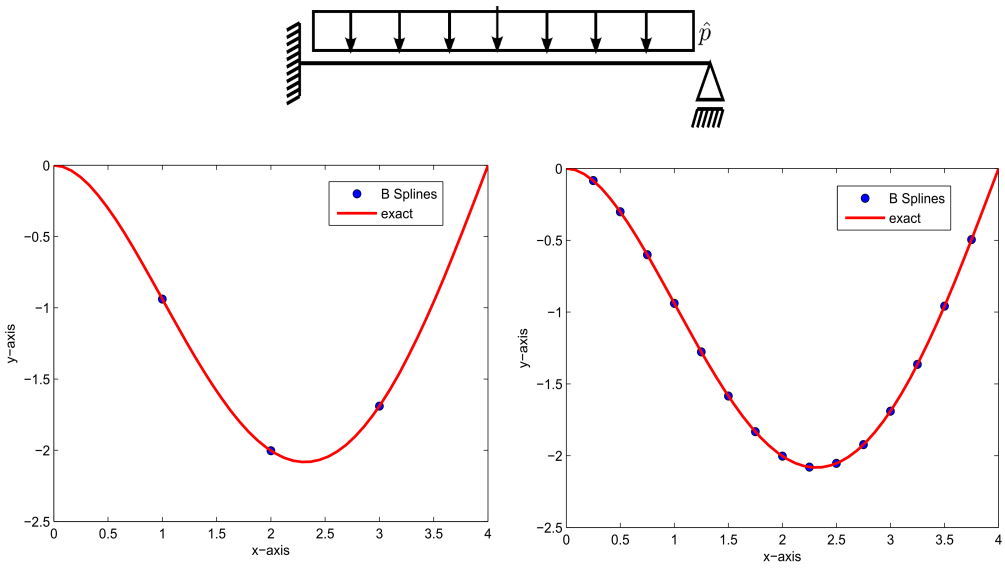

Figure 7.5: Clamped-Pinned: (a) mesh with 4 elements and (b) with 16 uniform elements

7.2 Nonlinear Problems

7.2.1 Truss

In order to validate the code for geometrically nonlinear problems, few examples were taken involving large deformations. First, the geometric nonlinear analysis of the truss member is performed and then analytically verified. The exact problem is illustrated in Fig 7.7. Both cases of uniform load $\hat{p}$ and point load $\hat{P}$ were taken one by one. For different values of α, the nonlinear truss was analyzed. The mesh used is depicted in Figure 7.6. Table 7.2 shows the end deflection after the nonlinear analysis for point load with both an uniform mesh of 4 elements. Table 7.3 shows for end deflection for uniform loading case. For both point and uniform loading, the deflection matches quite closely with the analytical values.

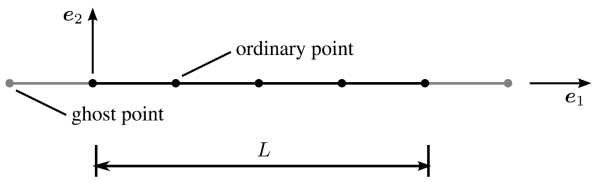

Figure 7.6: Uniform mesh for inclined truss

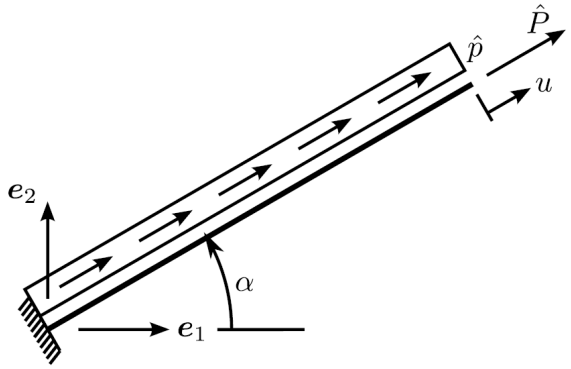

Figure 7.7: Inclined truss-geomterically nonlinear

System	α	Mesh:Figure 7.1(a)
Figure 7.5(a)	0	0.52138
Figure 7.5(b)	0	0.52138
Figure 7.5(a)	30	0.52138
Figure 7.5(b)	30	0.52138
Figure 7.5(a)	135	0.52138
Figure 7.5(b)	135	0.52138

Table 7.2: Results for E = 1000, A = 1, I = 1/12, $\hat{P} = 1000$, L = 1 ; reference solution $w = 0.52138$

System	Mesh	α
Figure 7.5(a)	0	0.30356
Figure 7.5(b)	0	0.30356
Figure 7.5(a)	30	0.30356
Figure 7.5(b)	30	0.30356
Figure 7.5(a)	135	0.30356
Figure 7.5(b)	135	0.30356

Table 7.3: Results for E = 1000, A = 1, I = 1/12, $\hat{p} = 1000$, L = 1 ; reference solution $w = 0.305428$

7.2.2 Buckling of Beam

Next, the problem of geometrically nonlinear beam buckling is taken. The problem is illustrated in Fig 7.8. Analytical methods can't be used in this case, in order to calculate the displacements at different load values. Instead, an incremental iterative procedure is followed, as it is typically done for nonlinear problems. Solutions of this type of nonlinear equations can be found iteratively by solving linearized equations, gradually

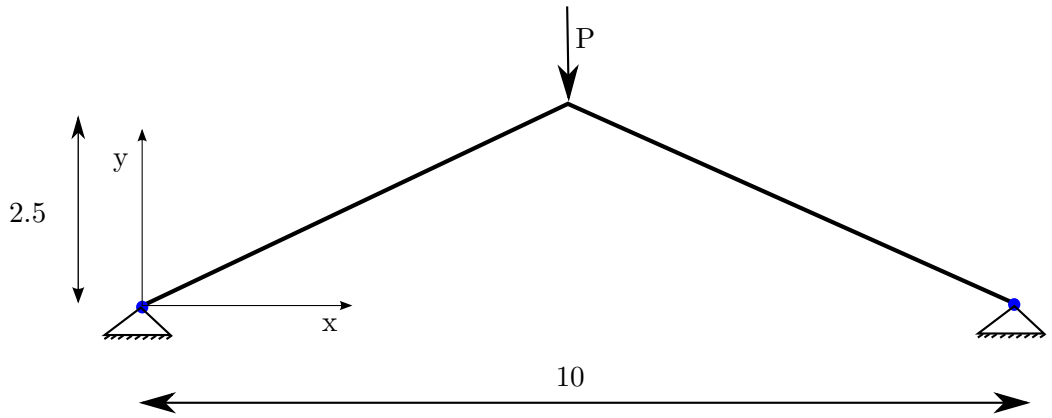

Figure 7.8: Geometry of bucking beam with E=10^5, h=0.01, L=10

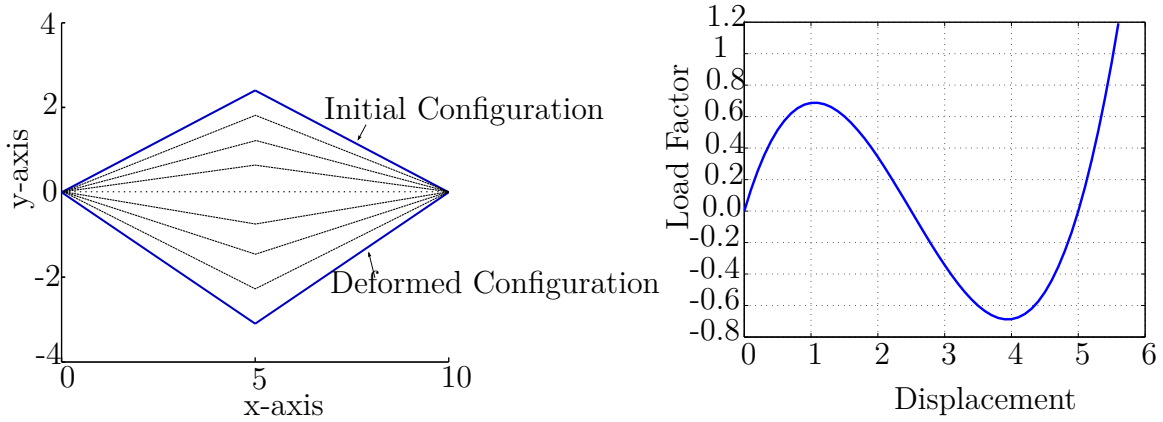

Figure 7.9: Buckling of Beam: a) Initial and Deformed Configuration b) Load Displacement Curve

approaching the displacement at equilibrium point. Newton Raphson method is used in general to solve the linearized equation, neglecting the higher order terms, to obtain a guess for a new displacement value. At each iteration, a better value of displacement is found, until convergence is reached, where the residual attains a very small value.

For this kind of problem, the displacement control is used where displacement is chosen as a control paramater at each step. Load displacement control would stop the simulation at the limit and turning point. Thus, the displacement control is more suitable for this kind of problem. However, other methods like arc length length could also be used. As, the main subject of this thesis is shape optimization, therefore more complex methodologies are not used for obtaining the load displacement curve. Using

displacement control method, therefore the resultant load deformation curve is then plotted in Figure 7.9 (b). The plot shows the snap through behaviour clearly in the load displacement curve. The initial and deformed shape of the beam with some intermediate displacements is also plotted in Fig 7.9 (a). The load deformation plot is quite as expected.

7.2.3 Buckling of Arch

Next, a problem of deep arch buckling was taken with non symmetrical loads. Figure 7.10 depicts the problem. Load deformation curve was plotted with both vertical load as well as horizontal load, as shown in Figure 7.11. The nonlinear analysis was performed using load control method.

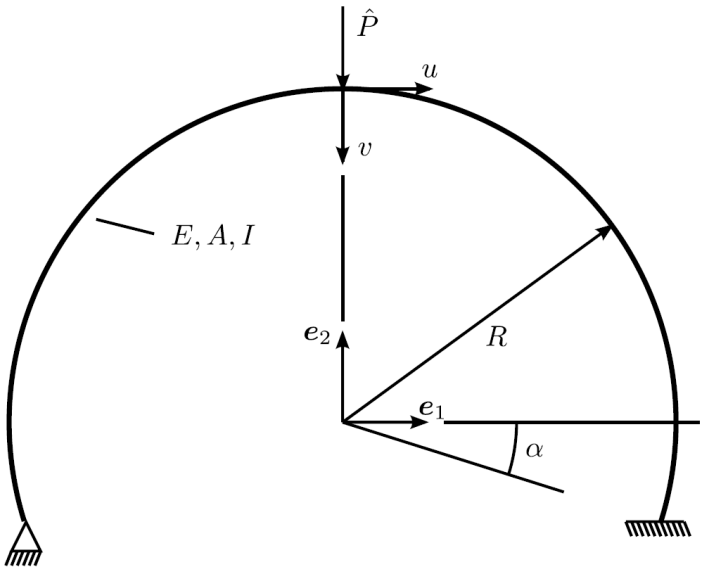

Figure 7.10: Deep arch with non-symmetric supports, E = $1.2 \cdot 10^7$ kN/cm^2, A = 1cm^2, I = 1/12 cm^4, R = 100cm, $\alpha = 17.5°$

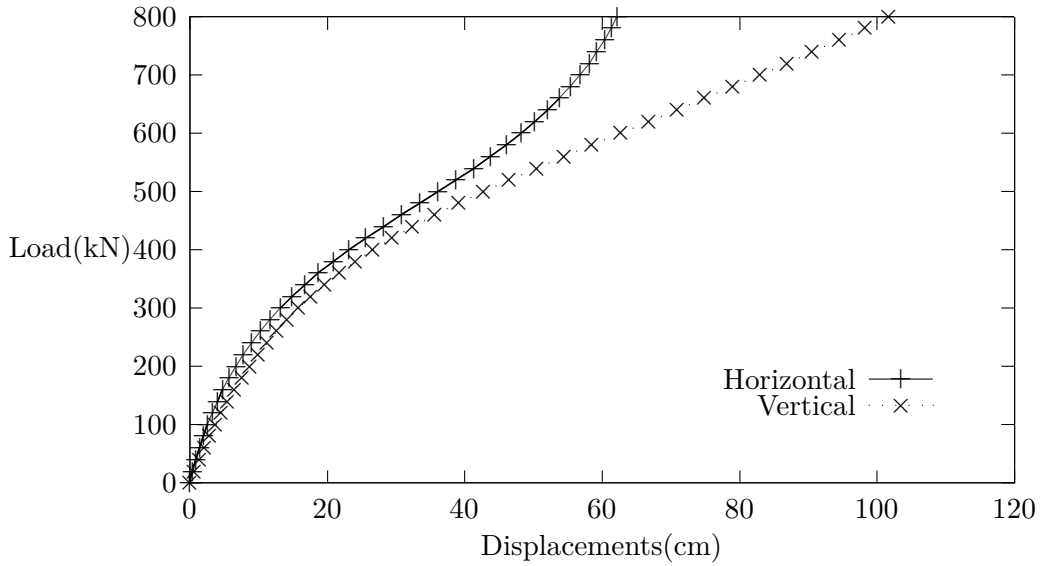

Figure 7.11: Load Displacement curve of Geometrical Nonlinear Arch

7.3 Shape Optimization

In this section, the sensitivities derived in Chapter 6 accounting for geometric nonlinearities in structure are used to find the optimized shape of the nonlinear structures. In all the numerical examples hereafter, the objective function is taken as Strain Energy, with the goal of minimizing it. The design variables are the control points of B-spline curve.

7.3.1 Catenary Curve: Verification problem

In this code verification example, a thin beam pinned at the ends is optimised for a vertical pressure load and compared with a catenary curve.
It has been known since the work of Leibniz, Huygens and Johann Bernoulli in 1691 that the shape of a curve assumed by a loose string hung freely from two fixed points is a catenary the general form of which is as follows:

$$y = \alpha cosh\left(\frac{x+\beta}{\alpha}\right) + \gamma \tag{7.7}$$

The unknown parameters α, β and γ are determined based on the location of the supports and length of the string l_0. The supports are at equal height and the horizontal distance between the supports is 10. Initially, the shape of beam is taken as straight connecting the supports with length equal to the distance between the supports. Width

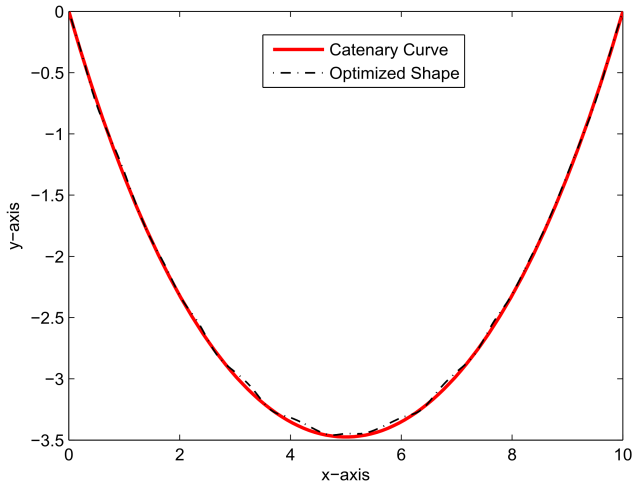

Figure 7.12: Comparision of the optimized shape with the catenary curve

and thickness are taken as constant, and doesn't change in the optimization process. As, it is in this example, a uniform loading of $p_y = -0.02$ is applied with the geometric properties as: E = 10^5, h=0.01, L=1000. It can been be seen that the catenary curve profile obtained using equation 7.7, and the optimized shape obtained for this conditions described matches quite well as shown in Figure 7.12. As the length by thickness ratio is very small (1000), there is significantly very small bending taking place, as a result the beam majorly has axial forces, making it ideal for validating with a catenary curve. Therefore the analytical sensitivities of a nonlinear beam problem is validated very well.

7.4 Effect of Optimized Shape by Changing Various Parameters

After validating the code with the example above, a study is made on how the optimized shape looks as various parameters are changes. Some conclusions and remarks are made at the end of each case.

7.4.1 Variation with Load

In case of a thin initially straight beam, a study is made for how the optimized shape looks like for different loads. As earlier, the objective function is minimizing the Strain Energy and the design variables are the B-spline control points. Initially, the optimized shape found for a very small load is shown in Figure 7.13. It is seen that as the load

is quite small, the optimized shape is close to the shape as it could be imagined for a linear case. This is obviously because the displacements are quite small, and falls in the linear regime of the load deformation curve. It is seen the cost funciton i.e the strain energy is reduced to about 73%.

Similarly for higher loads, the optimized shape is found in Figure 7.14, where the cost function decreses by 99.6% and in Figure 7.15 by 99.7%. In all the calculated optimized shapes, the cost functions thus reduces significantly.

It is quite clear that with the increasing load, the effect of nonlinearity is prominent and therefore a different shape is attained as expected from a linear case. In Figure 7.15, the shape goes in the positive y axis, because of the geometric nonlinear effects. Here, as the deformations are large, therefore, optimized shape calculated using linear sensitivities would not produce the most efficient shape. Hence, for large displacements, nonlinear analytical sensitivities are necessary and thus in this case this is how the optimized shape looks like.

For Point Load P at the center and the geometric properties as: E = 10^5, h = 0.01, L = 10

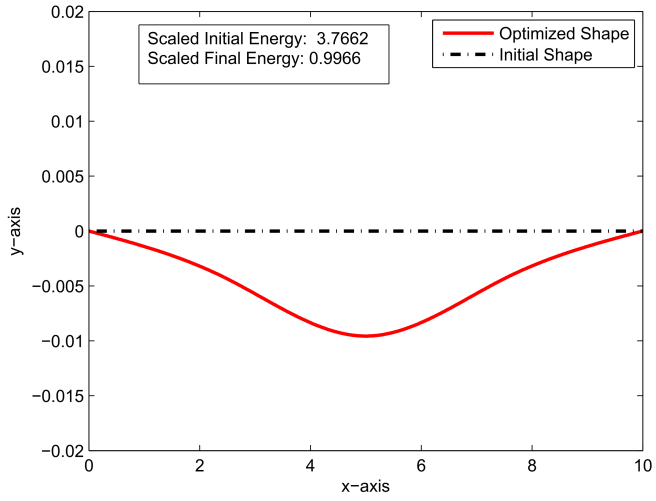

Figure 7.13: Initial and Optimized Shape for P=-2×10^{-5}

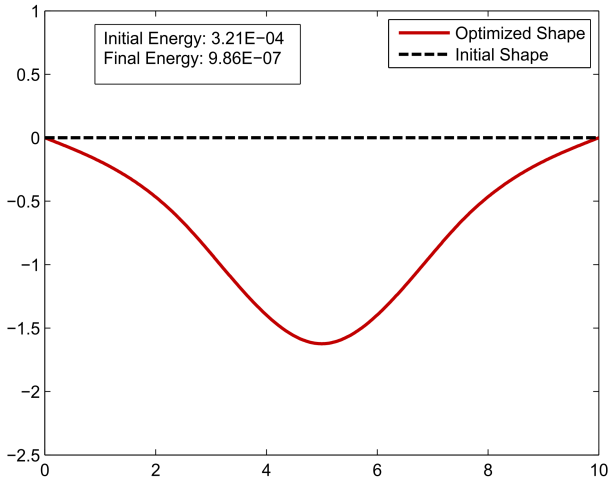

Figure 7.14: Initial and Optimized Shape for P=−0.02

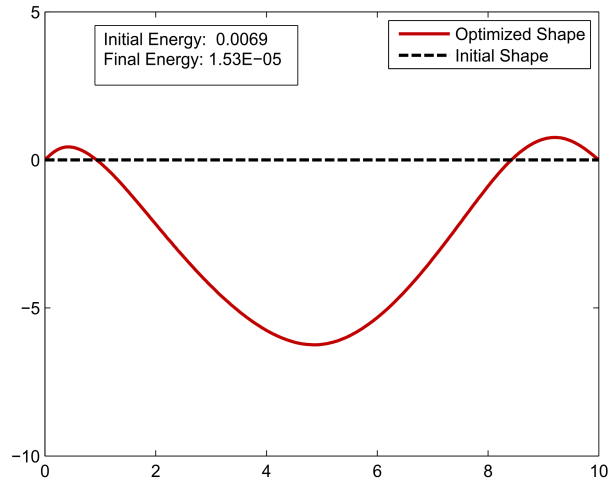

Figure 7.15: Initial and Optimized Shape for P=−0.2

7.4.2 Variation with Elements

In this example, a simply supported beam is taken with E = 10^5, h = 0.01, L = 10 and a point load P of −0.0005. Here also the objective function was taken as Strain Energy with the goal of minimizing it. The design variables are taken as the control points of the spline curve. Here, the optimal shape for the same problem is found using 8,16,32 elements as shown in Figure 7.16. The variation of the minimum cost function with the number of elements is plotted in the Figure 7.17. It is seen from Figure 7.17 that the cost at the optimal shape increses with increase in number of elements. This means that

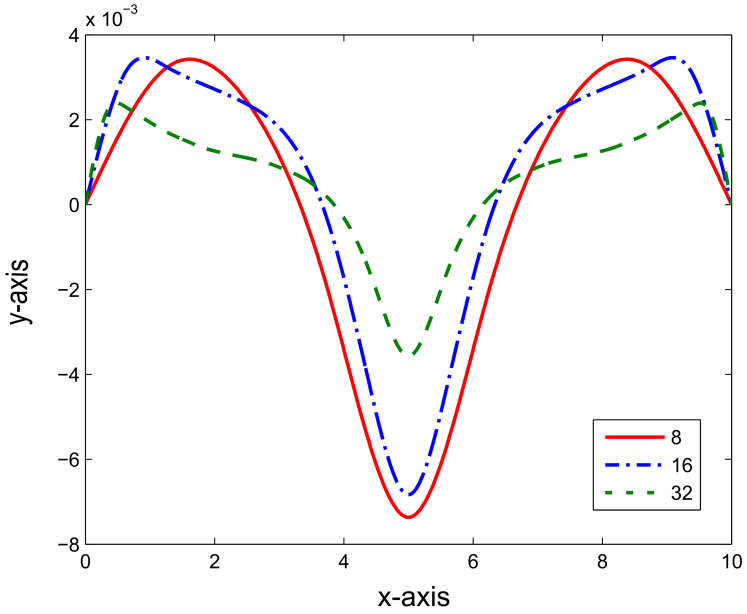

Figure 7.16: Initial and Optimized Shape for P=−0.2

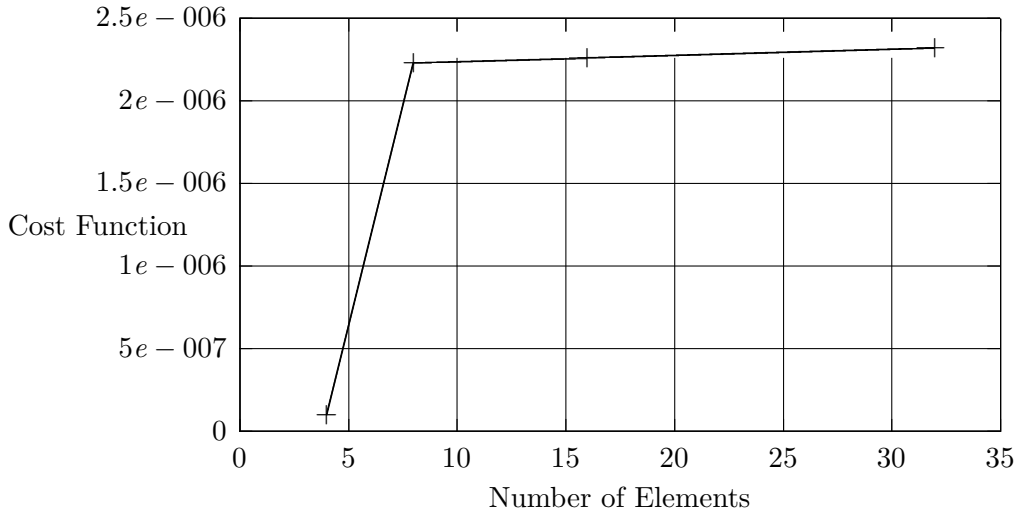

Figure 7.17: Variation of Minimum Cost Function with Number of Elements

for large number of elements, the optimization algorithm doesn't find a global minima, rather because of more discretization, the alogorithm stops finding some local minima solution. Only having the minimal number of design variables ensures convergence to the correct global minima.

7.4.3 Variation with L/t ratio

In this section, the effect of optimal shape in the geometrical nonlinear setting is investigated. A straight simple supported beam is taken with $E = 10^5$, and vertical point load as $P = -0.02$ was applied. The optimized shape was found for various L/t ratios and plotted in Figure 7.18. It can be seen that in a very thin beam i.e $L/t = 1000$, the beam is almost straight, with a kink near the ends. As compared to thicker beams, the optimal shape of a thinner beam has much larger length. It is quite reasonable as the deformation of the thin beam is larger and so optimal shape needs to have a larger length so that it is more stiffer. One point to note is that, with large deformations as in the case higher L/t ratio, the effect the nonlinearity is prominent. The obtained curve is not same with one would obtain for a linear case. Some part of the optimal curve is even going at the positive part of the y axis. But for a linear case, one would expect something like as shown in Figure 7.19. As for $L/t = 50$ where the displacements are smaller because to its thicker cros-ssection, the optimal shape is close to one would obtain for a linear case like in Figure 7.19. Obviously, a straight line could not be obtained, because the use of spline curve, and a curve type shape is inevitable. However, if more elements are used, a straighter shape could be obtained, but then in that case, the solution might tend to find a local minima as discussed in section 7.4.2.

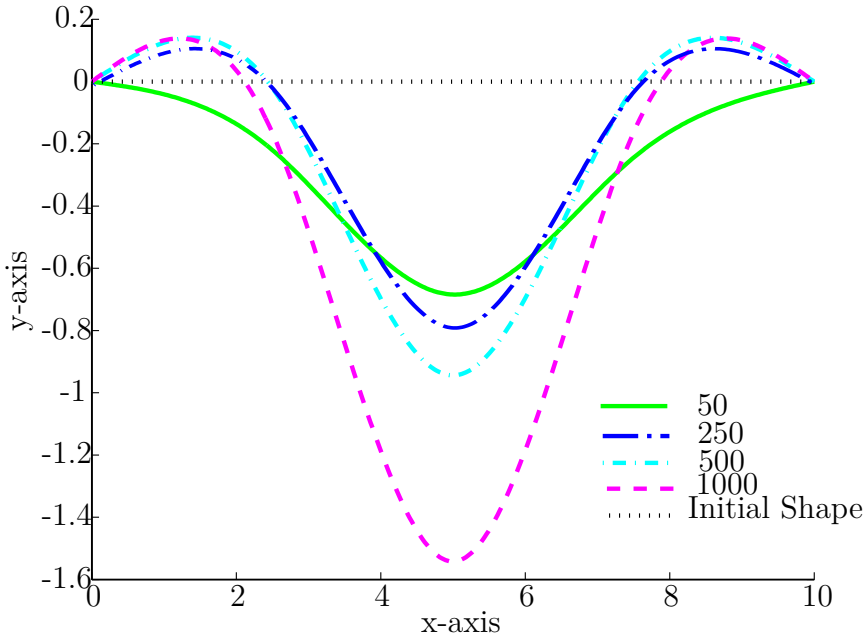

Figure 7.18: Optimal Shapes varying L/t ratio for point load

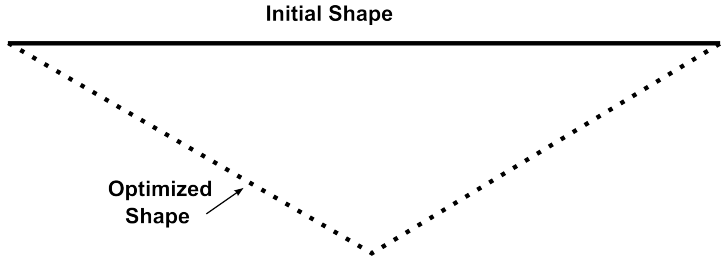

Figure 7.19: Optimal Shape expected for a point load in a linear case

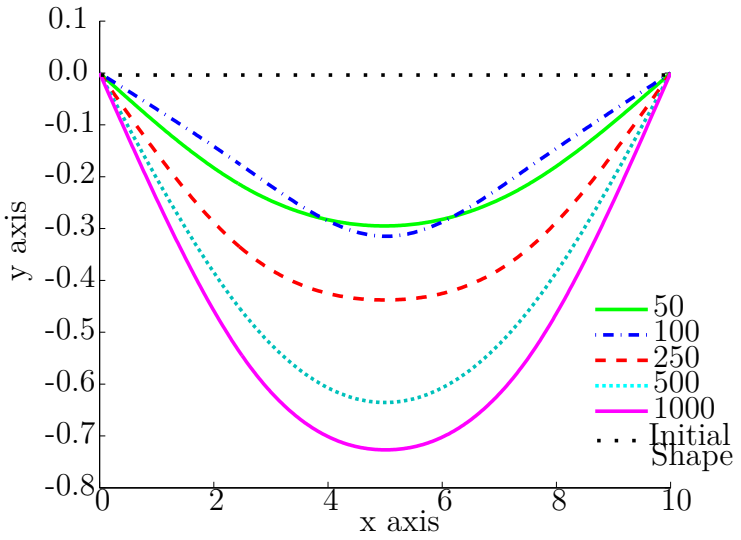

Figure 7.20: Optimal Shapes varying L/t ratio for uniform load

A similar investigation is also done for a uniform load case $p_y = -0.002$ with the same Elastic Modulus. Figure 7.20 shows optimal shapes for uniform load with varying L/t ratio. A similar argument could be given here also, and its quite clear that with lower L/t ratio, length of the optimal shape decreases. Table 7.4 and Table 7.5 depicts the initial and final cost and the percentage reduction for point load and uniform load respectively. In order to check, how the curves differ from the catenary curve which was calculated using equation 7.7, a comparison was made in Figure 7.21 for different L/t ratio. As expected, optimal shape of thin beam ($L/t = 1000$) has the same shape as that of the catenary curve. This is because for such a thin beam, the load is primarily carried by membrane effects. As the thickness is increased, the beam transfers more forces through bending action, as thus deviates from the catenary curve profile. Thus, it could be said that the catenary curve profile doesn't proves to be a good validation for the optimized shape in case of thicker beams, but behaves very well with thin beams.

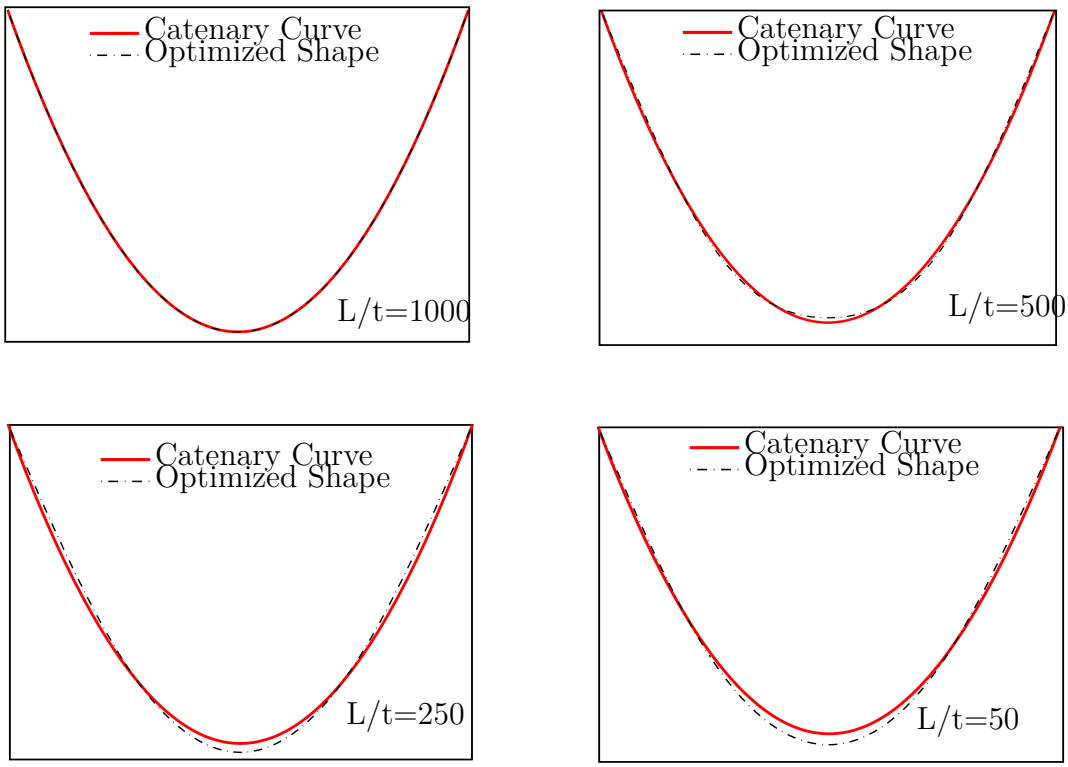

Figure 7.21: Comparison of Optimal Shapes at different L/t ratio with the respective catenary curve. The red line depicts the catenary curve and the dotted black line the optimal shape,initially the beam is considered straight

L/t	Initial Cost	Final Cost	% Cost Reduction
50	8.4123e-6	2.498e-7	97.03
100	6.54e-5	1.317e-7	99.79
250	2.3757e-4	8.311e-8	99.96
500	2.6488e-4	9.99e-7	99.62
1000	3.2076e-4	9.867e-7	99.69

Table 7.4: Variation of cost function with L/t ratio for point load

L/t	Initial Cost	Final Cost	% Cost Reduction
50	3.713e-6	2.188e-7	94.10
100	3.07e-5	7.480e-7	97.56
250	1.433e-4	5.488e-8	99.96
500	1.576e-4	6.178e-7	99.61
1000	1.89e-4	3.985e-7	99.78

Table 7.5: Variation of cost function with L/t ratio for uniform load -0.02

7.4.4 Buckling of Beam

The nonlinear analysis of a thin beam was performed in Section 7.2.2 and the load displacement curve was illustrated in Figure 7.9(b). A total load of 35 was applied, and it was seen that the limit point was near to load of 20. Now, the optimal shape of the beam was found for increasing load as shown in Figure 7.22. It was seen that for load very near to the limit point, there was drastic change the height of the optimal shape. This is quite expected as for higher loads the optimal shape should have a high stiffness, for which it attains a much larger height that loads below the limit point. This also makes sense, as the structure after the limit becomes softer and undergoes the snap through phenomenon, involving large deformation. Having a initial shape as found will result in minimum strain energy at this loading. It is also seen that the attained optimal shape follows a symmterical geometry.

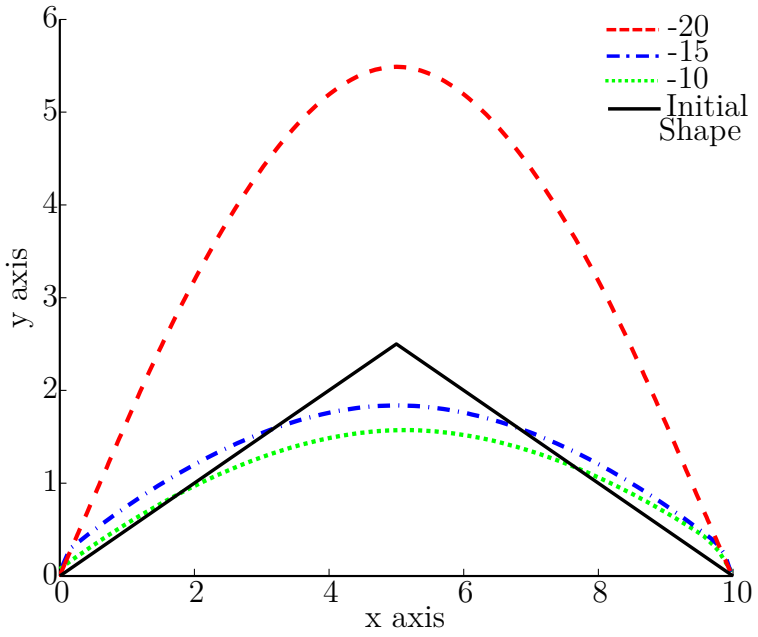

Figure 7.22: Optimal Shapes of at Various Load Points

8

Summary and Outlook

The analytical sensitivity was computed for a nonlinear beam in a parameter free space. The exact and smooth geometric representation inherent in the isogeometric analysis model is included into the shape optimization process merging analysis and design model. Since the geometry is encapsulated at the design level, mesh refinement and representation of shape changes are easily obtained without the need of subsequent communication of CAD enviroment. This framework not only unifies geometry and analysis, but is superior over standard polynomial based finite element analysis from numerical aspect with precise representation of complex geometries, reducing geometric error and higher order inter element continuity. A isogeometric analysis of linear as well as nonlinear beam was performed and was compared with the analytical results. Even for very small number of elements, results are very close to the analytical ones.

Next, for the optimization of the nonlinear beam, the analytical sensitivities were calculated. The objective was to minimize the strain energy with design variable as the control points of B-Spline mesh. The adjoint method was adopted for discrete sensitivity analysis, which is more efficient from computational point of view, as in this case the number of design variables are more than the reponse functions. Once the sensitivities were calculated for the objective function, it was feeded to the optimization algorithm in MATLAB. In this work, the interior point method was used, as it quite efficient for nonlinear optimization problems.

The whole algorithm is illustrated in Fig 8.1 and is discussed below:

1. Initially a guess is made for the design variables i.e control points of the B-Spline curve

2. With this initial configuration, the beam problem is solved by Newton Raphson iterations until the residual become zero. The displacements found are added iteratively. Finally, the equilibirium state of the beam is found.
3. Once the equilibirium position is attained, the value of the objective function i.e. Strain Energy is calculated at the current state.
4. The nonlinear sensitivity of the nonlinear beam is then calculated using the formulation followed in Chapter 6.
5. Once, the objective function and its sensitivity is computed, it is feeded to the optimization algorithm which then finds another better initial configuration.
6. This is then again feed into the Newton raphson loop and 1-5 is followed again until the final optimized shape is obtained.

Using this algorithm, the optimized shape was found out for various problems. Some validation was done on the lines of inverted catenary curve usually used in architecture. The concept used is that the inverted catenary curve gives the most optimized shape for structures in pure membrane stress state. Therefore, a comparison was made with the optimal shape for a uniform loading considering geometrically nonlinear behaviour and the catenary curve. It was seen that for very thin beams, both the curves matched closely. However, with the increase in thickness, it was seen deviation with the catenary curve profile. This is because now due to increase in bending stiffness, the beam doesn't carry load in pure membrane action.

Further, it was also investigated how the the optimal shape looks when the load was increased for both uniform and point loads. For all the loads, there was significant amount of cost reduction.

Another interesting study was done, on how the optimal shape varied with change in number of elements, or the mesh size. It was found out that, with the increase in number of elements, the solution tends to find some local minima. Only having minimal number of design variables, ensure convergence to the correct global minima, thus producing exact optimal shapes. Similar behaviour was also found for shape optimization of shells by Bletzinger et al. (1993)

The variation of optimal shape with change in L/t ratio was also studied. First, with point loads, it was seen that for thicker beams i.e smaller L/t ratio, the optimal shape looked similar the shape as expected for a linear case. This was because, the displacement was small in that case and the beam was still in the linear regime. As the L/t ratio was increased, there was prominent deviation from the linear optimal shape because of large beam deformations. For uniform loads, the variation with L/t ratio was compared with the respective catenary curve. It was seen that catenary curve profile doesn't

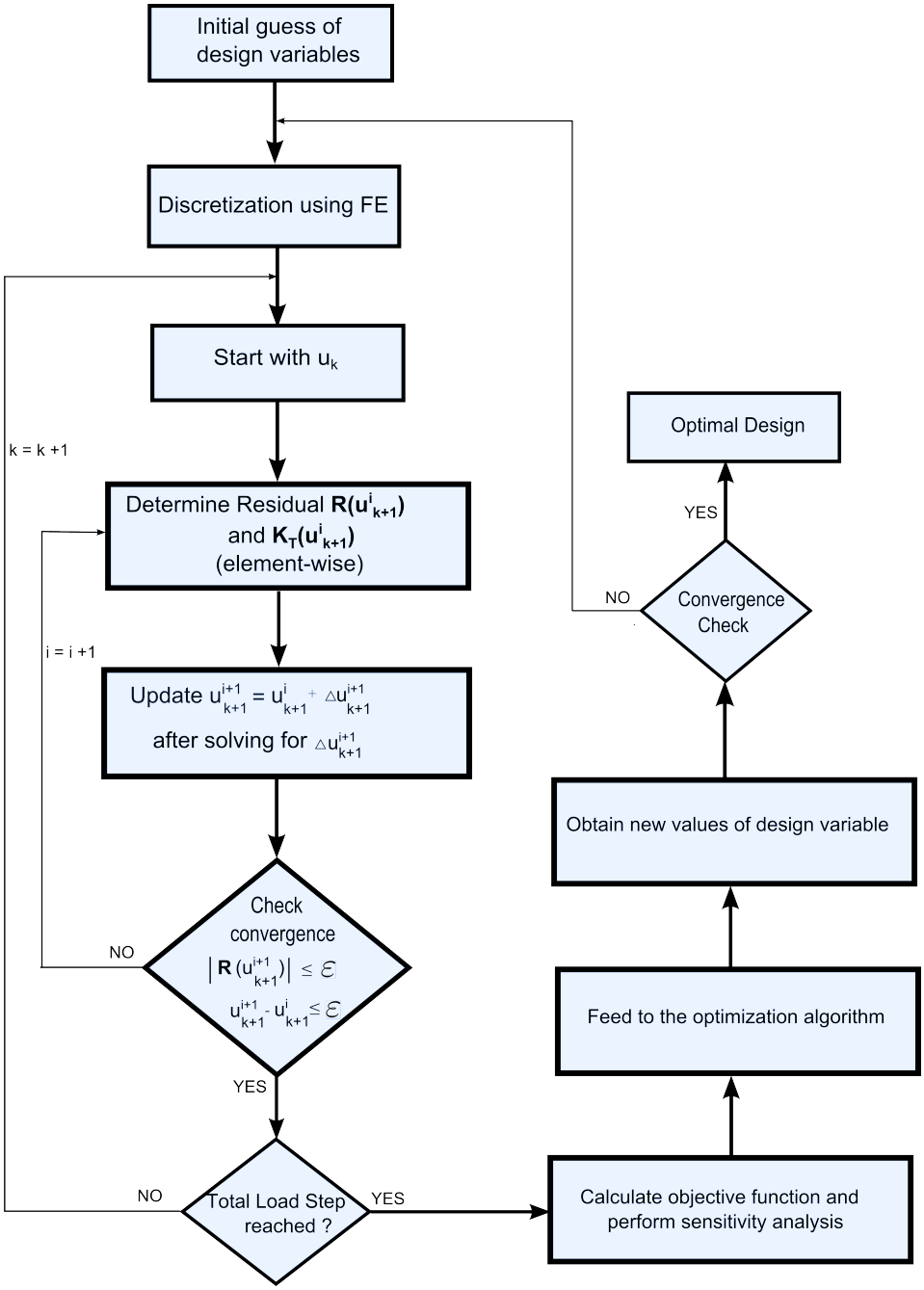

Figure 8.1: Flowchart for nonlinear shape optimization

proves to be a good validation for the optimized shape in case of thicker beams, but behaves very well with thin beams. Thus the catenary curve profile is a good validation for geometric nonlinear beams but only with thinner cross-section.

Finally, the optimized shape was found for a beam buckling with a point load at the centre. The geometrical nonlinear analysis was first performed and the load deformation

curve was plotted. With this the limit point of the beam was also found. The optimized shape was then found for increasing loads till the load where limit point was attained. It was seen that for load very near to the limit point, there was drastic increase in the height of the optimal shape. This is quite expected as near the limit point the beam becomes more soft and thus with increase in the height, the stiffness of the beam increases. Through all these numerical studies, the shape optimization for nonlinear structures thus was very well studied, and a general behaviour of how the optimal shape varies on changing beam parameters was also demonstrated.

This approach surely involves higher mathematical complexity but is much more efficient and has lower computational costs that global finite differences and semi-analytical methods. However, in order to reach a higher load state in the nonlinear analysis, the computation is quite expensive in order to find the optimal shape design. Therefore, there is research scope of finding more efficient algorithms for calculating the sensitivities involving large nonlinearity.

As the beam formulation used is based on the thin shell formulation, this framework would be easily extended to shape optimization of nonlinear shells.

It is also possible to further exploit the potential idea of isogeometric elements. Optimized design could be found my using NURBS based represention, T-Splines. It could be also extended by using subdivision surfaces.

Further, material nonlinearities could be taken into account for more realistic shape designs.

Thus, with these capabilities incorporated in the present model, complex and realistic systems requiring nonlinear analysis can be designed for optimum performance, which has always been the foremost goal of all design engineers.

Bibliography

Bletzinger et al. 1993
: Bletzinger, K.U.; Wall; Ramm, E.: Form finding of shells by structural optimization. In: *Engineering with Computers* 9 (1993), S. 27–35

Block et al. 2006
: Block, P.; DeJong, M.; Ochsendorf, J.: As Hangs the Flexible Line:Equilibrium of Masonry Arches. In: *Nexus Network Journal* 8 (2006), S. 13–24

Braibant and Fleury 1984
: Braibant, V.; Fleury, C.: Shape Optimal Design using B-Splines. In: *Computer Methods in Applied Mechanics and Engineering* 44 (1984), S. 247–267

Cho and Ha 2009
: Cho, S.; Ha, S.H.: Isogeometric shape design optimization: exact geometry and enhanced sensitivity. In: *Struct Multidisc Optim* 38 (2009), S. 53–70

Cho and Jung 2003
: Cho, S.; Jung, H.S.: Design sensitivity analysis and topology optimization of displacement–loaded non-linear structures. In: *Computer Methods in Applied Mechanics and Engineering* 192 (2003), S. 2539–2553

Cirak et al. 2000
: Cirak, F.; Ortiz, M.; Schröder, P.: Subdivision surfaces:A new paradigm for thin-shell finite-element analysis. In: *International Journal for Numerical Methods in Engineering* 47 (2000), S. 379–393

Cirak et al. 2002
Cirak, F.; Scott, M.J.; Antonsson, E.K.; Ortiz, M.; Schröder, P.: Integrated modeling, finite-element analysis and engineering design for thin-shell structures using subdivision. In: *Computer-Aided Design* 34(2) (2002), S. 137–148

Firl 2010
Firl, M.: *Optimal Shape Design of Shell Structures*, Lehrstuhl für Statik der Technischen Universität München, Dissertation, 2010

Ha et al. 2010
Ha, S.H.; Choi, K.K.; Cho, S.: Numerical method for shape optimization using T-spline based isogeometric method. In: *Struct Multidisc Optim* 42 (2010), S. 417–428

Haftka and Grandhi 1986
Haftka, R. T.; Grandhi, R. V.: Structural Shape Optimization-A Survey. In: *Computer Methods in Applied Mechanics and Engineering* 57 (1986), S. 91–106

Heymann 1995
Heymann, J.: *El esqueleto de piedra. Mecánica de la arquitectura de fábrica.* Cambridge University Press, 1995

Isler 2000
Isler, H.: Creating shell shapes . Bridge between civil engineering and architecture:procedueres. In: *Proceedings of Structural morphology colloquium,Delft University of Technology*, 2000

Larena 2009,Cottbus
Larena, A.B.: Shape Design Methods Based on the Optimisation of the Structure. Historical Background and Application to Contemporary Architecture. In: *Proceedings of the Third International Congress on Construction History*, 2009,Cottbus

Mehrotra 1992
Mehrotra, S.: On the Implementation of a Primal-Dual Interior Point Method. In: *SIAM J. Optimization* 3 (1992), S. 575–601

Olhoff and J. 1991
Olhoff, N.; J., Rasmussen: Study of inaccuracy in semi-analytical sensitivity analysis — a model problem. In: *Structural optimization* 3 (1991), S. 203–213

Pedersen and Laursen 1983
Pedersen, P.; Laursen, C.L.: Design for Minimum Stress Concentration by Finite Element and Linear Programming. In: *Journal of Structural Mechanics* 10 (1983), S. 375–391

Qian 2010
Qian, X.: Full Analytical Sensitivities in NURBS based Isogeometric Shape Optimization. In: *Computer Methods in Applied Mechanics and Engineering* 199 (2010), S. 2059–2071

Santos and Choi 1992
Santos, J.L.T; Choi, K.K: Shape design sensitivity analysis of nonlinear structural systems. In: *Structural optimization* 4 (1992), S. 23–35

Schramm and Pilkey 1993
Schramm, U.; Pilkey, W.D.: The coupling of geometric descriptions and finite elements using NURBs-A study in shape optimization. In: *Finite Elements in Analysis and Design* 15 (1993), S. 11–34

Wall et al. 2008
Wall, W.A.; Frenzel, M.; Cyron, C.: Isogeometric structural shape optimization. In: *Comput. Methods Appl. Mech. Engrg.* 197 (2008), S. 2976–2988

Weisstein
Weisstein, Eric W.: "Interior Point Method." From MathWorld–A Wolfram Web Resource. In: *http://mathworld.wolfram.com/InteriorPointMethod.html*

Zienkiewicz and Campbell 1973
Zienkiewicz, O. C.; Campbell, J. S.: Shape optimization and linear programming. In: *Optimum Structural Design* 19 (1973), S. 1249–1263

Appendix

Derivative of a normalized vector

Consider a vector

$$\mathbf{v} = \frac{\mathbf{v}^*}{|\mathbf{v}^*|} \tag{1}$$

The partial derivative with respect to any variable s is given by:

$$\mathbf{v}_{,s} = \frac{\mathbf{v}^*_{,s}|\mathbf{v}^*| - \mathbf{v}^*|\mathbf{v}^*|_{,s}}{|\mathbf{v}^*|^2} \tag{2}$$

where

$$|\mathbf{v}^*|_{,s} = \frac{\mathbf{v}^* \cdot |\mathbf{v}^*|_{,s}}{|\mathbf{v}^*|} \tag{3}$$

Derivative of magnitude of a vector

The magnitude of a vector $\mathbf{v}^*$ is given by:

$$|\mathbf{v}^*| = \sqrt{\mathbf{v}^* \cdot \mathbf{v}^*} \tag{4}$$

and the derivative of this magnitude with respect to s can be written as:

$$||\mathbf{v}^*|_{,s} = \frac{\mathbf{v}^* \cdot |\mathbf{v}^*|_{,s}}{|\mathbf{v}^*|} \tag{5}$$

Derivative of a cross product

The cross product of two vectors $\mathbf{a}(s)$ and $\mathbf{b}(s)$ is given by:

$$\mathbf{a} \times \mathbf{b} = \begin{pmatrix} a_2 b_3 - a_3 b_2 \\ a_3 b_1 - a_1 b_3 \\ a_1 b_2 - a_2 b_1 \end{pmatrix}$$

where a_i and b_i are the i^{th} component of the vectors $\mathbf{a}$ and $\mathbf{b}$ respectively.
The derivative of the cross product with respect to the variables s can be written as:

$$(\mathbf{a} \times \mathbf{b})_{,s} = \begin{pmatrix} (a_2)_{,s} b_3 - (a_3)_{,s} b_2 + a_2 (b_3)_{,s} - a_3 (b_2)_{,s} \\ (a_3)_{,s} b_1 - (a_1)_{,s} b_3 + a_3 (b_1)_{,s} - a_1 (b_3)_{,s} \\ (a_1)_{,s} b_2 - (a_2)_{,s} b_1 + a_1 (b_2)_{,s} - a_2 (b_1)_{,s} \end{pmatrix}$$

$$= \begin{pmatrix} a_2 (b_3)_{,s} - a_3 (b_2)_{,s} \\ a_3 (b_1)_{,s} - a_1 (b_3)_{,s} \\ a_1 (b_2)_{,s} - a_2 (b_1)_{,s} \end{pmatrix} + \begin{pmatrix} (a_2)_{,s} b_3 - (a_3)_{,s} b_2 \\ (a_3)_{,s} b_1 - (a_1)_{,s} b_3 \\ (a_1)_{,s} b_2 - (a_2)_{,s} b_1 \end{pmatrix}$$

$$= (\mathbf{a}_s \times \mathbf{b}) + (\mathbf{a} \times \mathbf{b}_s) \tag{6}$$

In (6) it can be said that the product rule applies for the cross product.